Electronic Supplementary Information

Structure-directing effect of Terephthalate bridging Zn(II)- and Cd(II)-based coordination polymers towards application for the detection of trace quantity of Pd²⁺ in aqueous medium and their electrical conductivities

Koushik Saha,[a] Basudeb Dutta,[a,b] Pubali Das,[c] Angeera Chandra,[a] Arnab Samanta,[d] Sudeep Ranjan Jana,[a] Sudip Naskar,[e] Rajat Saha,[f] Partha Pratim Ray[c] and Chittaranjan Sinha*[a]

[a]Department of Chemistry, Jadavpur University, Kolkata 700032, West Bengal, India.

[b] Institute for Integrated Cell-Material Sciences, Kyoto University, Yoshida Ushinomiya-cho, Sakyo-ku, Kyoto 606-8501, Japan

[c]Department of Physics, Jadavpur University, Kolkata 700032, West Bengal, India.

[d]Department of Chemical Sciences, Indian Institute of Science Education and Research Kolkata, Mohanpur, West Bengal 741246, India.
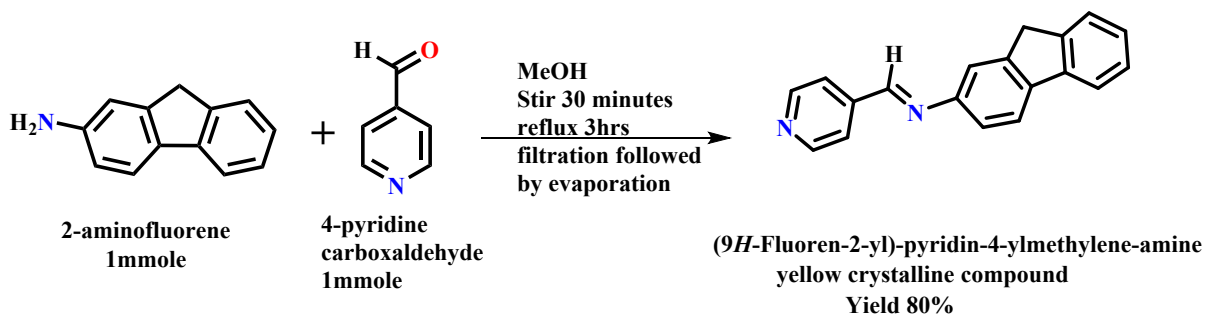
[e] Quantum Materials & Devices Unit, Institute of Nano Science and Technology, Knowledge City, Sector 81, Mohali 140306, India

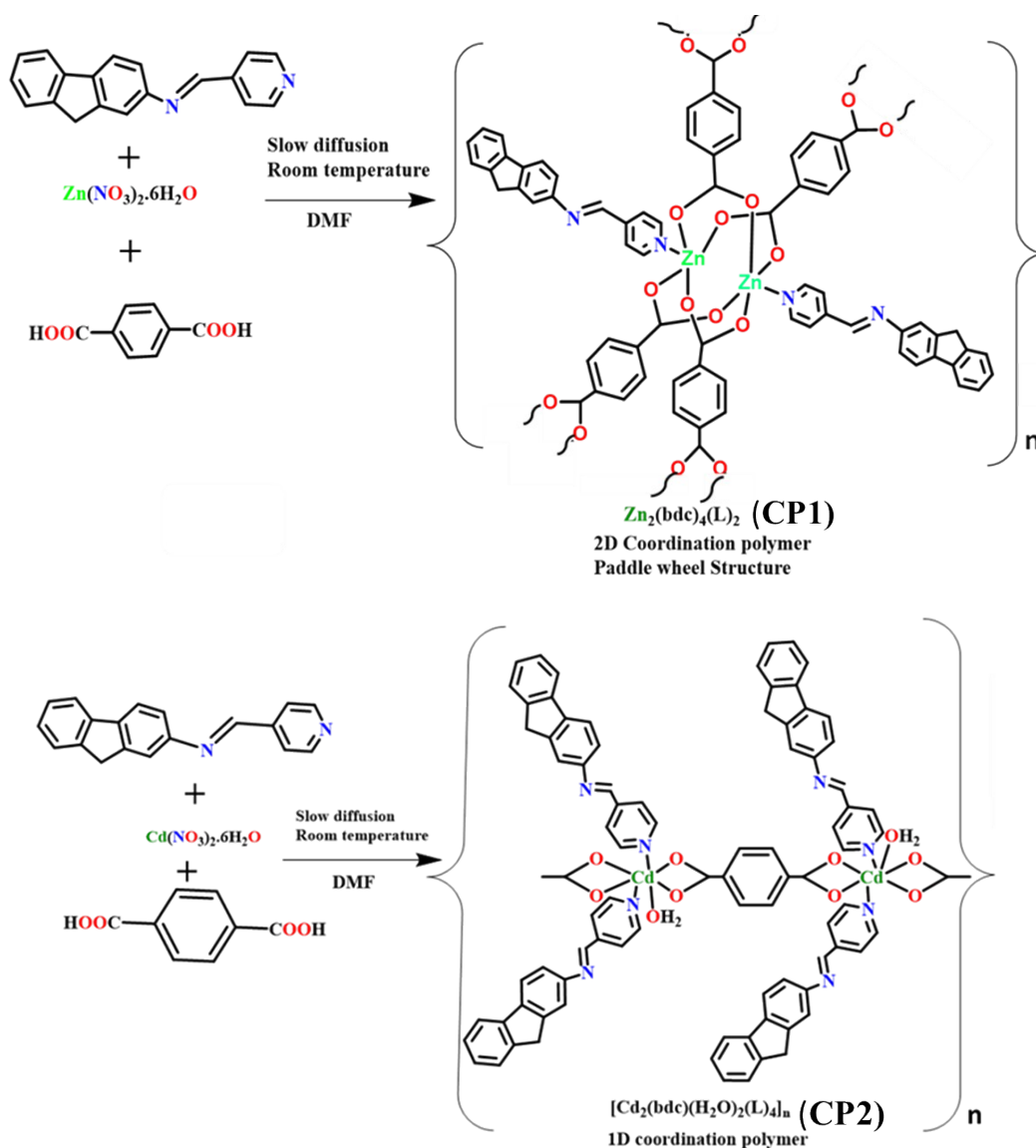[f] Department of Chemistry, Kazi Nazrul University, Asansol 713340, India

To whom it may correspondence: crsjuchem@gmail.com

Sl. No.	Contents	Page No.
1.	**Scheme 1**. Synthesis of 9H-Fluoren-2-yl)-pyridin-4-ylmethylene-amine **(flpy)**	**4**
2.	**Scheme 2**. Synthesis of **CP1** and **CP2**	**4**
3.	**Figure S1**. Mass spectrum of **flpy**	**5**
4.	**Figure S2**. ^{1}H NMR spectrum of **flpy** in DMSO-d_6	**5**
5.	**Figure S3**. ^{13}C NMR spectrum of **flpy** in DMSO-d_6	**6**
6.	**Figure S4 & S5**. FTIR spectra of (a) **CP1** and (b) **CP2** in absence and presence of Pd^{2+}.	**6- 7**
7.	Materials and General method	**7- 8**
8.	Preparation of the Schiff base Ligand (**flpy**)	**8**
9.	Structure Determination by X-ray.	**9**
10.	**Table S1, S2 &S2.** Crystallographic data, Bond lengths and bond angles and $\pi \ldots \pi$ interaction related data of **CP1**.	**9-11**
11.	**Table S4, S5 &S6.** Crystallographic data, Bond lengths and bond angles and $\pi \ldots \pi$ interaction, H-bonding interaction related data of **CP2**.	**12-14**
12.	**Figure S6 & S7.** View of supramolecular assemble; Coordination polyhedral around the constituting central metal of **CP1** and various interaction of **CP2**.	**15**
13.	**Figure S6.** TGA plots of **CP1** and **CP2**.	**16**
14.	**Figure S9.** Powder X-ray Diffraction analysis of **CP1** and **CP2**.	**16**
15.	UV-Visible and Fluorescence Spectral Experiments	**16-17**
16.	**Figure S10.** UV-Visible spectrum of **flpy, CP1** and **CP2**	**17**
17.	**Figure S11.** Absorption spectra of **CP1**(a) and **CP2**(b) dispersed in aqueous medium in presence of different metal ions.	**18**
18.	**Figure S12.** Emission Intensity of **CPS** in absence and presence of Pd^{2+}	**18**
19.	Sensing Experiment and Detection limit calculation of both CPs for Pd (II)	**18-19**
20.	**Figure S13.** Stern-Volmer plot at lower range of **CP1** and **CP2**.	**19**
21.	**Figure S14.** Limit of detection plot and calculation of detection limit of **CP1** and **CP2** for Pd(II).	**20**
22.	**Figure S15.** Stern-Volmer plot of **CP1** and **CP2**.	**20**
23.	**Figure S6.** Emission intensity of CPs and [CPs+Pd^{2+}] at different pH range (2 to 12).	**20**
24.	**Figure S17.** IR spectra of CPs at different pH	**21**

Scheme S1. Synthesis of (9H-Fluoren-2-yl)-pyridin-4-ylmethylene-amine (**flpy**).

Scheme S2. Synthesis of $[Zn_2(bdc)_4(flpy)_2)]_n$ (**CP1**), $[Cd_2(bdc)_2(flpy)_4(H_2O)_2]_n$ (**CP2**).
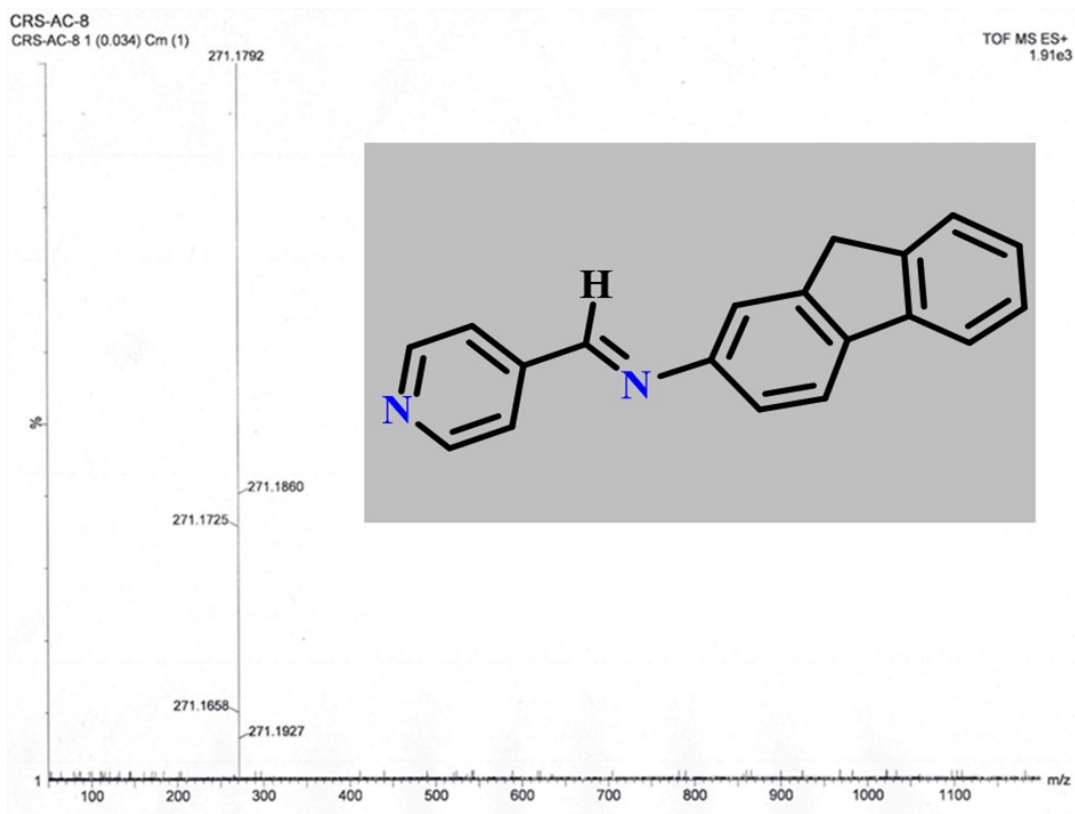
Figure S1. Mass spectrum of **flpy.**
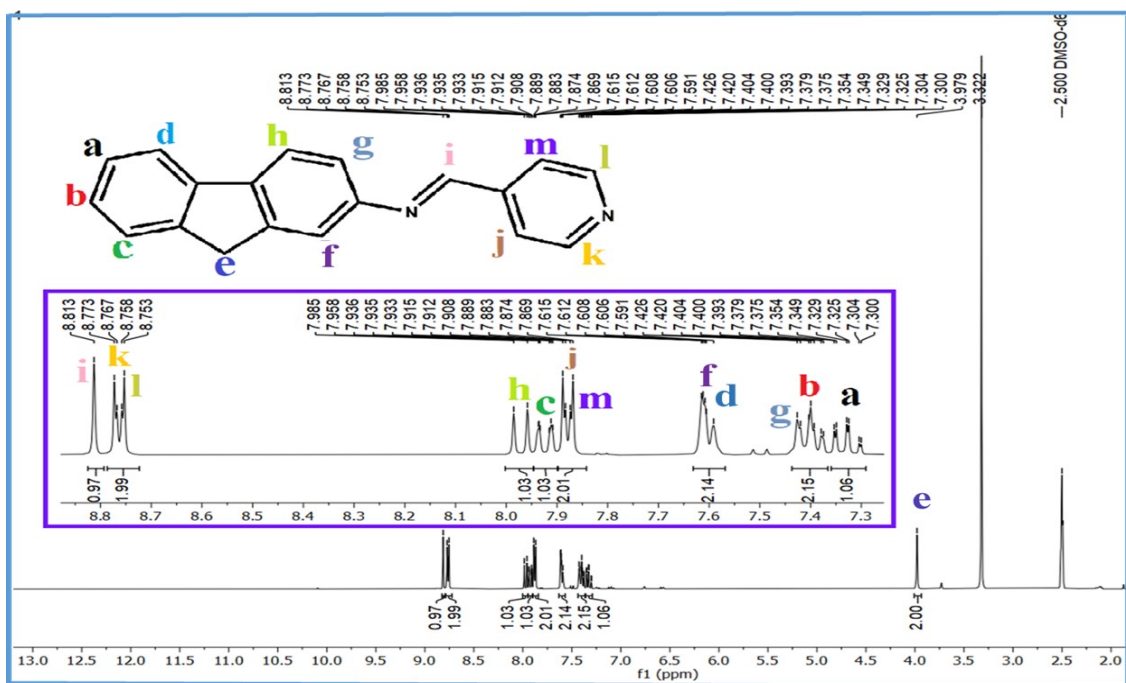

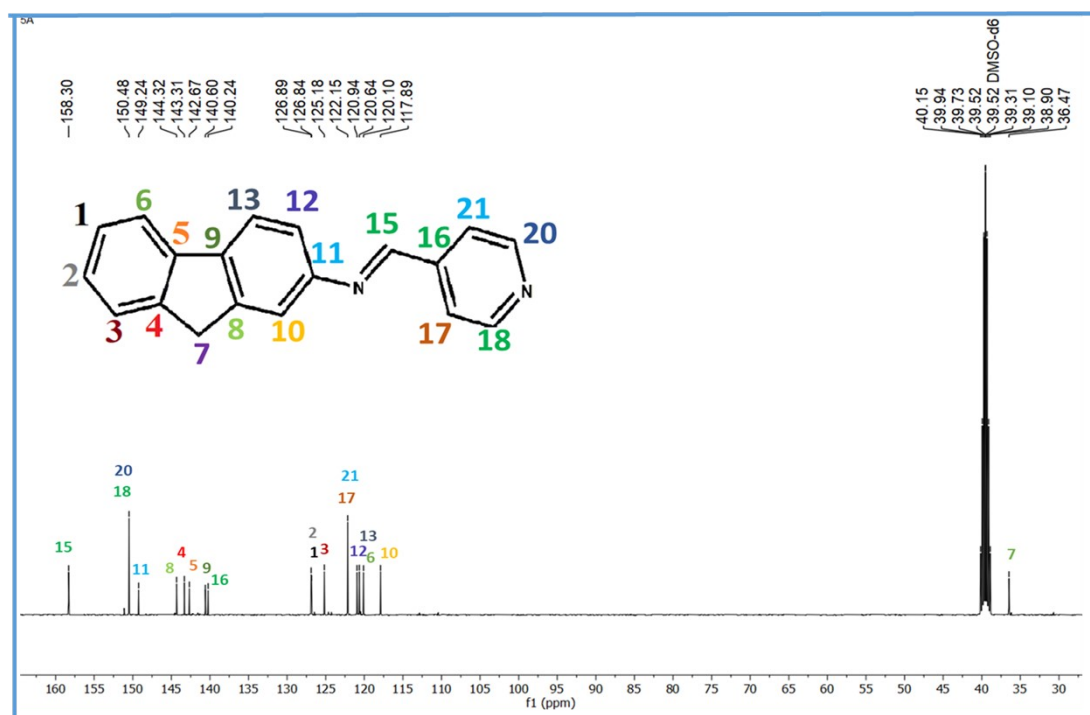**Figure S2.** ^{1}H-NMR spectrum of **flpy** in DMSO-d$_{6}$

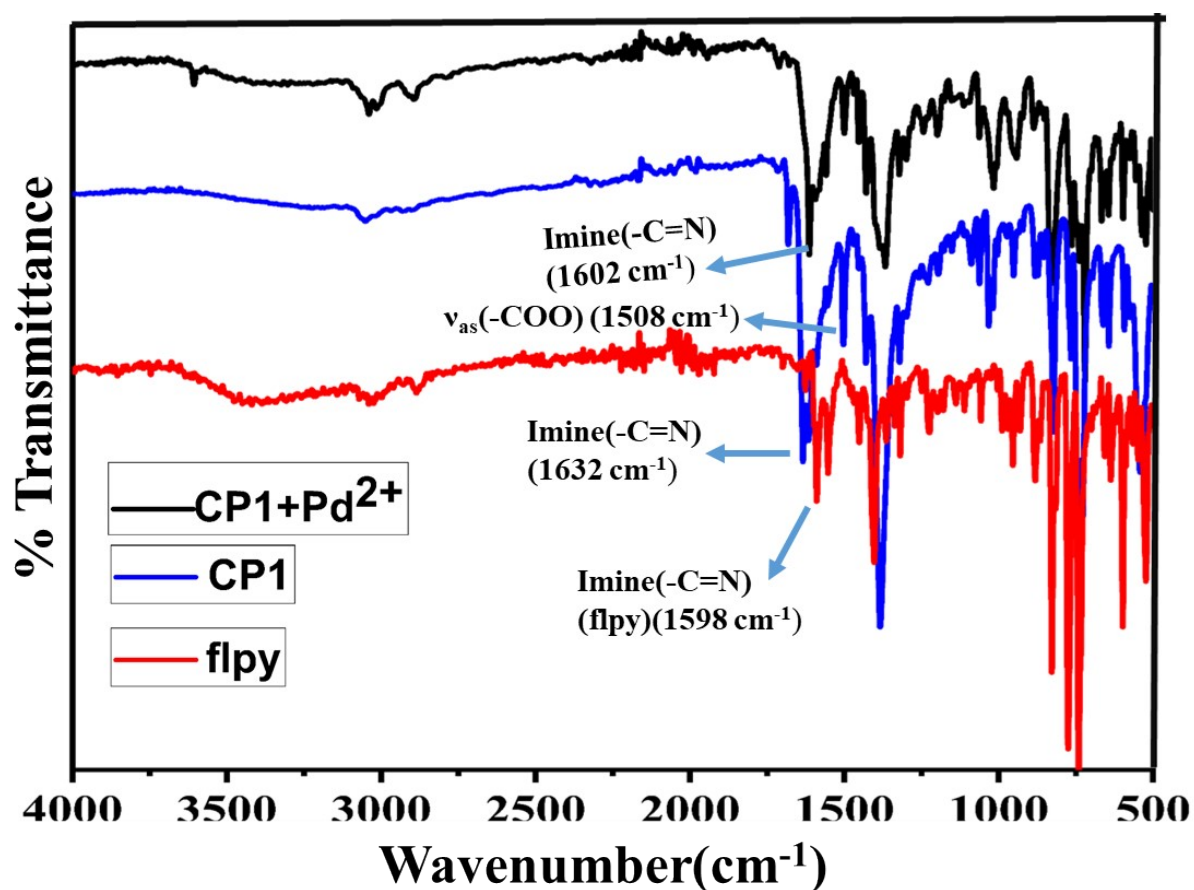**Figure S3.** ^{13}C-NMR spectrum of **flpy** in DMSO-d$_6$

Figure S4. FTIR spectra of **flpy**(red); **CP1**(blue) and **CP1** in presence of Pd^{2+}(black).
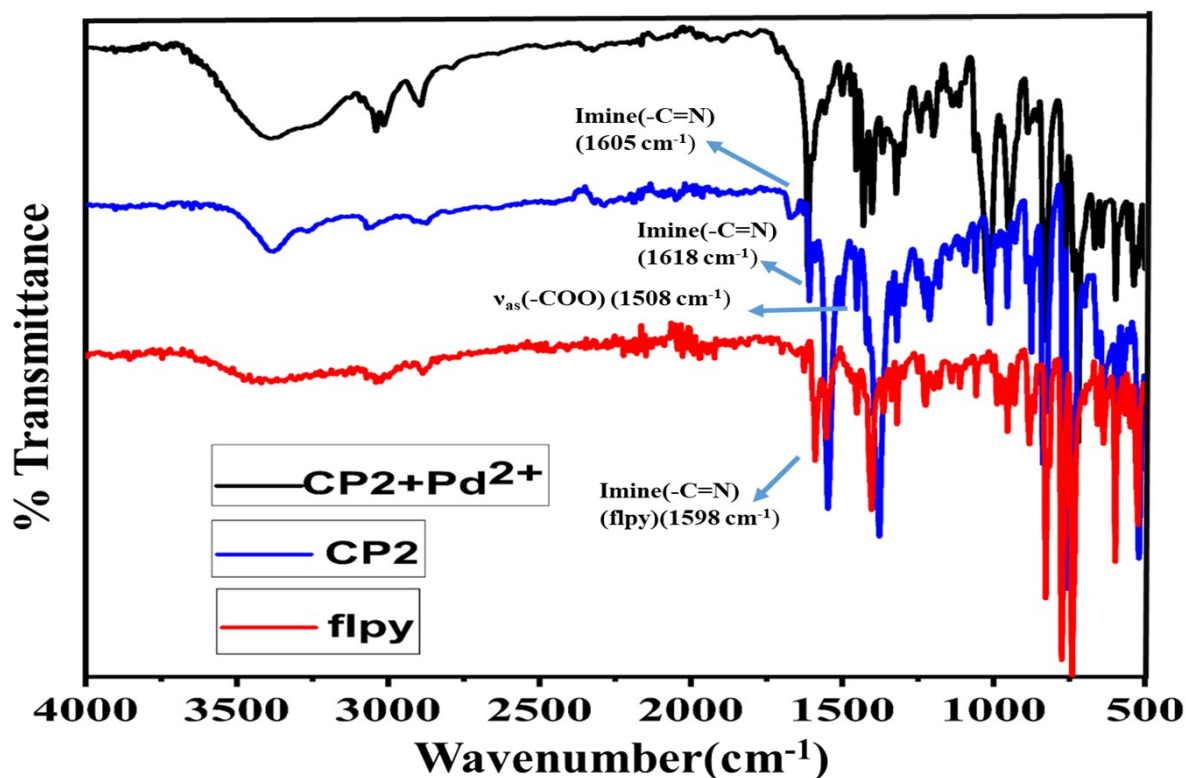
Figure S5. FTIR spectra of **flpy** (red); **CP2** (blue) and **CP2** in presence of Pd^{2+}(black).

Materials and General Method

$Zn(NO_3)_2 \cdot 6H_2O$, $Cd(NO_3)_2 \cdot 4H_2O$, 4-Pyridinecarboxaldehyde, 2-Aminofluorene were procured from Sigma-Aldrich. 1,4-Benzene dicarboxylic acid (H$_2$**bdc)** and other reagents were collected from Merck, India and used without further purification. Thin layer chromatography (TLC) plates (Merck silica gel 60, f254) were applied to guide the reaction. To represent ^{1}H-NMR spectra in DMSO-d^6 solvent on 300 MHz (Bruker-DPX) and 400 MHz (JEOL-JNM-ECZ400S/L1) NMR instruments were utilized and tetramethylsilane (TMS) was used as an internal standard. ^{13}C NMR spectra were depicted on 75 MHz (Bruker D8 high-resolution mass spectrometry PX) and 100 MHz spectrometers (JEOL JNM-ECZ400S/L1) in DMSO-d^6 solvents using tetramethylsilane (TMS) as the internal standard. For CHN analysis, a PerkinElmer 240C elemental analyzer was utilized. PerkinElmer Spectrum II LITA FT-IR spectrometer was handled to collect the infrared spectrum (4000–500 cm^{-1}). A Perkin Elmer Pyris Diamond TG/DTA instrument was exploited to test the thermal stability of the as-synthesized compound in a temperature range between 30°C and 800°C at a heating rate of 10°C

min^{-1}. Operating a Pyris Diamond Thermogravimetric Analyzer (TGA), the thermal stability of the coordination polymer was evaluated. Ambient temperature X-ray powder diffraction (XRPD) patterns were collected on a Bruker D8 ADVANCE X-ray diffractometer using Cu Kα radiation (λ = 1.548 Å) produced at 40 kV and 40 mA at a 2θ range of 5−50°. A FEI-built Field Emission Scanning Electron Microscope (FESEM) (Inspect F50) image was exert to testify the morphological characterization via FESEM micrograph. EDS (Energy Dispersive X-ray Spectra) was required to identify the elemental analysis. The ESI technique with a Q-Tof Micro mass spectrometer was utilised to measure HRMS (m/z). Fluorescence and UV−vis spectra were evaluated by exploiting on a PerkinElmer spectrofluorometer model LS55 and PerkinElmer Lambda 25 spectrophotometer, respectively. Fluorescence lifetime measurement has been done by Horiba Jobin Yvon Fluorescence Spectrophotometer.

Preparation of the Schiff base Ligand (flpy)

The synthesis of Schiff-bases ligand, 9H-Fluoren-2-yl-pyridin-4-ylmethylene-amine **(flpy)** was carried out by usual condensation reaction **(Scheme S1, ESI†)** by adding 4-Pyridinecarboxaldehyde (107 mg, 1.0 mmol) dropwise to methanolic solution (10.0 ml) of 2-Aminofluorene (181.23 mg, 1.0 mmol) in a round-bottom flask with continuous stirring and refluxed the mixture for about 6 h. Completion of the reaction was confirmed by thin layer chromatography (TLC) and the reaction mixture was cooled down to ambient condition. The solvent was removed by using a rotary evaporator under vacuum. The faint yellow compound of the Schiff base, **flpy** was observed and dried for further experimentation (Yield: 0.36 g, 80%) **(SchemeS1)**. HRMS (ESI, m/z): calcd. for $C_{19}H_{14}N_2$ [M + H]$^+$: 271.1191; found: 271.1792 **(Figure S1)**; ^{1}H NMR (300 MHz, DMSO) δ 8.81 (s, 1H), δ 8.81 (s, 1H), 8.77- 8.75 (m, 2H), 7.97 (d, J = 8.1 Hz, 1H), 7.94 – 7.91 (m, 1H), 7.91-7.87 (m, 2H), 7.62 – 7.59 (m, 2H), 7.43 – 7.38 (m, 2H), 7.33 (td, J = 7.5, 1.2 Hz, 1H), 3.98 (s, 2H) **(Figure S2)** (s = singlet, d = doublet, t = triplet, m = multiplet); ^{13}C NMR (300 MHz, CDCl$_3$): δ 158.30, 150.48, 149.24, 144.32, 143.31, 142.67, 140.60, 140.24, 126.89, 126.84, 125.18, 122.15, 120.94, 120.64,

120.10, 117.89, 36.47 (**Figure S3**); IR($\bar{v}$): 3100 cm^{-1}, $\bar{v}$(=C-H); 1598 cm^{-1}, $\bar{v}$ (imine –CH=N–) **(Figure S4).**

Structure Determination by Single Crystal X-Ray Diffraction Analysis

To obtain the X-ray data, both the single crystals having a proper dimension (**CP1**: 0.25 x 0.19 x 0.15 mm^3; **CP2**: 0.10 x 0.20 x 0.20 mm^3) of **CP1** and **CP2** were selected from the solution, dipped in oil, and mounted on a goniometer head by using a Bruker SMART APEX II CCD diffractometer furnished with a graphite-monochromated MoKα radiation source (λ = 0.71073 Å) for **CP1** at 273 K and Cu Kα radiation source (λ = 1.54184) for **CP2**. The unit cell parameters and crystal-orientation matrices were calculated using least squares refinements of all reflections in the hkl range, specifically, -13 ≤ h ≤ 13, -14 ≤ k ≤ 14, -14 ≤ l ≤ 14 (**CP1**) and -15 ≤ h ≤ 14, -26 ≤ k ≤ 26, -27 ≤ l ≤ 46 (**CP2**) respectively. Due to Lorentz and polarization effects, the intensity data were modified by using Reflections accessible in the 2θmax range with the SAINT program.[S1] The crystallographic data **(Table S1&S4)** were used for integration (I > 2σ(I)) and SADABS [S2,S3] was used for absorption correction. SHELXT 2014/5 package helped to solve the single crystal structure and refinement was carried out using Olex2 1.5-dev. [S4] Anisotropic thermal parameters plays compatible role to refine the non-hydrogen atoms of the compound. Hydrogen atoms of the compound molecular system were located in their geometrically perfect positions and inhibited to ride over their parent atoms. For **CP1**, there are some electron densities located close to the binuclear paddle-wheel cluster which are chemically irrelevant. So, we did not consider them during structure analysis.   The designated bond lengths and bond angles are labelled in **CP1(Table S2)** and in **CP2(Table S5)**. CCDC number for former compounds are: 2336302 and 2336301 respectively.

Table S1. Crystal data and refinement parameters for **CP1**.

Formula	$C_{27}H_{18}N_2O_4Zn$
CCDC	2336302
Formula weight	499.82
Crystal system	Triclinic
space group	P -1
a (Å)	10.8901
b (Å)	10.9435
c (Å)	11.3604
α (deg)	110.319
β (deg)	100.038
γ (deg)	98.351
V (Å^3)	1218.8
Z	2
D_{calcd}(g/cm3)	1.362
μ (mm^{-1})	1.042
λ (Å)	0.71073
data[$I > 2\sigma$ (I)]/params	5337/307
GOF on F^2	1.146
h, k, l	13,14,14
final R indices[$I > 2\sigma(I)$][a,b]	$R1 = 0.0524$ $wR2 = 0.1715$

[a]$R1 = \Sigma\|F_o\|$ $\|F_c\|/ \Sigma\|F_o\|$, [b]$wR2 = [\Sigma w(F_o^2$ $F_c^2)^2/\Sigma w(F_o^2)^2]^{1/2}$

Table S2. Selected bond lengths and bond angles in **CP1**.

Zn(1) - O(1)	2.042(5)	O(1) - Zn(1) - O(3)	89.07(18)
Zn(1) - O(3)	2.014(3)	O(1) - Zn(1) - N(1)	99.84(18)
Zn(1) - N(1)	2.033(4)	O(1) - Zn(1) - O(2)b	159.94(17)
Zn(1) - O(2)b	2.055(4)	O(1) - Zn(1) - O(4)b	88.84(18)
Zn(1) - O(4)b	2.035(4)	O(3) - Zn(1) - N(1)	102.06(17)

O(1) - C(24)	1.254(7)	O(3) - Zn(1) - O(2)b	88.64(18)
O(2) - C(24)	1.261(7)	O(3) - Zn(1) - O(4)b	159.03(17)
O(3) - C(20)	1.249(6)	N(1) - Zn(1) - O(2)b	100.13(18)
O(4) - C(20)	1.252(6)	N(1) - Zn(1) - O(4)b	98.86(17)
N(1) - C(1)	1.320(8)	O(2)b - Zn(1) - O(4)b	86.23(18)
N(1) - C(5)	1.334(8)	Zn(1) - O(1) - C(24)	131.0(4)
N(2) - C(6)	1.237(9)	C(24) - O(2) - Zn(1)b	123.0(3)
N(2) - C(7)	1.423(7)	Zn(1) - O(3) - C(20)	123.9(3)
Zn(1) - N(1) - C(5)	119.7(4)	C(20) - O(4) - Zn(1)b	131.1(3)
C(1) - N(1) - C(5)	116.7(5)	Zn(1) - N(1) - C(1)	123.2(4)
C(6) - N(2) - C(7)	121.4(6)	N(1) - C(1) - C(2)	123.8(6)
N(1) - C(5) - C(4)	122.9(6)	N(2) - C(7) - C(19)	115.7(5)
N(2) - C(6) - C(3)	120.8(6)	O(3) - C(20) - O(4)	125.3(4)
N(2) - C(7) - C(8)	124.6(5)	O(3) - C(20) - C(21)	117.6(4)
O(4) - C(20) - C(21)	117.1(4)		

Table S3. π … π interaction related data of **CP1**.

π … π interaction		
Ring(i) → Ring(j)	Distance between the (i, j) ring centroids (Å) in the crystal	[ARU(j)]
Cg(5)→ Cg(3)	3.70 Å	[1454.01]
Cg(3)→ Cg(3)	3.897	[2555.01]
Cg(1)→ Cg(5)	3.796	[2666.01]
Cg(5)→ Cg(4)	4.27 Å	[1454.01]
Cg(2)→ Cg(4)	4.278	[2555.01]

Where, Cg2= [N(1) –C(1) –C(2) –C(3) –C(4) –C(5)] of the pyridine ring ,[Cg3= C(7) – C(8) – C(9) – C(10) – C(18) – C(19)] and [Cg4= C(11) – C(12) – C(13) – C(14) – C(15) – C(16)] of fluorene moiety in flpy ,[Cg5 = C(21) – C(22) – C(23) – C(21)c – C(22)c –C(23)c] benzene ring of H_2bdc rings.

Table S4. Crystal data and refinement parameters for **CP2.**

Formula	$C_{65}H_{45}N_6O_5Cd$
CCDC	2336301
Formula weight	1102.47
Crystal system	Orthorhombic
space group	P b c a
a (Å)	12.1334(2)
b (Å)	21.5349(3)
c (Å)	38.1513(5)
α (deg)	90
β (deg)	90
γ (deg)	90
V (Å^3)	9968.6(3)
Z	8
D_{calcd}(g/cm3)	1.469
μ (mm^{-1})	4.007
λ (Å)	1.54184
data[$I > 2\sigma$ (I)]/params	9985/677
GOF on F^2	1.056
h, k, l	14,26,46
final R indices[$I > 2\sigma(I)$]^{a,b}	$R1 = 0.0492(7887)$ $wR2 = 0.1511(9985)$

$^aR1 = \Sigma||F_o|$ $|F_c||/ \Sigma|F_o|$, $^bwR2 = [\Sigma w(F_o{}^2$ $F_c{}^2)^2/\Sigma w(F_o{}^2)^2]^{1/2}$

Table S2. Selected bond lengths and bond angles in **CP2.**

Cd(1) - O(1)	2.434(2)	O(4) - C(46)	1.256(3)
Cd(1) - O(2)	2.378(2)	N(1) - C(1)	1.345(4)
Cd(1) - O(5)	2.252(2)	N(1) - C(5)	1.337(4)
Cd(1) - N(1)	2.364(3)	N(2) - C(6)	1.263(5)

Cd(1) - N(3)	2.356(3)	N(2) - C(7)	1.424(5)
Cd(1) - O(3)b	2.407(2)	N(3) - C(20)	1.336(4)
Cd(1) - O(4)b	2.406(2)	N(3) - C(24)	1.348(4)
O(1) - C(39)	1.261(4)	N(4) - C(25)	1.265(4)
O(2) - C(39)	1.258(5)	N(4) - C(26)	1.420(4)
O(3) - C(46)	1.264(3)	O(2) - Cd(1) - N(3)	96.60(10)
O(1) - Cd(1) - O(2)	54.32(10)	O(2) - Cd(1) - C(39)	27.18(11)
O(1) - Cd(1) - O(5)	135.86(8)	O(2) - Cd(1) - O(3)b	144.27(10)
O(1) - Cd(1) - N(1)	85.57(9)	O(2) - Cd(1) - O(4)b	160.10(10)
O(1) - Cd(1) - N(3)	89.45(9)	O(2) - Cd(1) - C(46)b	171.36(10)
O(1) - Cd(1) - C(39)	27.29(9)	O(5) - Cd(1) - N(1)	96.18(10)
O(1) - Cd(1) - O(3)b	90.12(8)	O(5) - Cd(1) - N(3)	91.57(10)
O(1) - Cd(1) - O(4)b	144.49(8)	O(5) - Cd(1) - C(39)	108.95(10)
O(1) - Cd(1) - C(46)b	117.57(7)	O(5) - Cd(1) - O(3)b	133.94(8)
O(2) - Cd(1) - O(5)	81.77(11)	O(5) - Cd(1) - O(4)b	79.63(8)
O(2) - Cd(1) - N(1)	85.35(10)	O(5) - Cd(1) - C(46)b	106.51(8)
N(1) - Cd(1) - N(3)	172.22(8)	N(1) - Cd(1) - C(39)	82.81(9)
N(1) - Cd(1) - O(3)b	88.96(8)	N(1) - Cd(1) - O(4)b	89.64(10)
N(1) - Cd(1) - C(46)b	91.21(9)	N(3) - Cd(1) - C(39)	95.47(9)
N(3) - Cd(1) - O(3)b	85.07(8)	N(3) - Cd(1) - O(4)b	90.96(9)
N(3) - Cd(1) - C(46)b	85.79(9)	C(39) - Cd(1) - O(3)b	117.10(9)
C(39) - Cd(1) - O(4)b	169.07(9)	C(39) - Cd(1) - C(46)b	144.46(9)
O(3)b - Cd(1) - O(4)b	54.58(7)	O(3)b - Cd(1) - C(46)b	27.45(7)
O(4)b - Cd(1) - C(46)b	27.26(7)	Cd(1) - O(1) - C(39)	90.45(19)
Cd(1) - O(2) - C(39)	93.1(2)	C(46) - O(3) - Cd(1)a	91.14(17)
C(46) - O(4) - Cd(1)a	91.43(17)	Cd(1) - N(1) - C(1)	120.2(2)
Cd(1) - N(1) - C(5)	122.6(2)	C(1) - N(1) - C(5)	117.1(3)
C(6) - N(2) - C(7)	121.0(3)	Cd(1) - N(3) - C(20)	121.0(2)
Cd(1) - N(3) - C(24)	121.9(2)	N(1) - C(5) - C(4)	123.0(3)

N(1) - C(1) - C(2)	123.9(3)	N(2) - C(6) - C(3)	122.1(3)
N(2) - C(7) - C(8)	115.4(3)	Cd(1) - C(39) - O(2)	59.71(16)
Cd(1) - C(39) - C(40)	171.39(19)	Cd(1) - C(39) - O(1)	62.26(16)
O(4) - C(46) - Cd(1)a	61.31(15)	C(43) - C(46) - Cd(1)a	171.33(19)

Table S6. π …π interaction and H-bonding interaction related data of **CP2.**

π … π interaction		
Ring(i) → Ring(j)	Distance between the (i, j) ring centroids (Å) in the crystal	[ARU(j)]
Cg(2)→ Cg(10)	3.640 Å	[8564.02]
Cg(2)→ Cg(12)	3.782Å	[8564.02]
Cg(3)→ Cg(6)	3.808Å	[5666.01]
Cg(4)→ Cg(11)	3.682 Å	[8564.02]
Cg(1)→ Cg(3)	3.808 Å	[5666.01]
Cg(7)→ Cg(12)	3.828 Å	[8564.02]
Cg(8)→ Cg(10)	3.778 Å	[8564.02]
Cg(8)→ Cg(13)	3.709 Å	[8565.01]
Cg(8)→ Cg(13)	3.709 Å	[8565.01]

Where, Cg 1 = C (9)- C (10) - C (11) - C (16) - C (17), Cg 3 = N (1) - C (1) - C (2) - C (3) - C (4) - C (5)

Cg 2 = C (29) – C (30) - C (35) - C (36) - C (37), Cg 4 = N(3) - C(20) - C(21) - C(22) - C(23) - C(24)

Cg 6 = C(11) - C(12) - C(13) - C(14) - C(15) -C(16), Cg 7 = C(26) - C(27) - C(28) - C(29) - C(37) - C(38) - C(30)

Cg 8 = C(31) - C(32) - C(33) - C(34) - C(35), Cg 10 = C(57) - C(58) - C(63) - C(64) - C(65),

Cg 11 = N (6) – C (48) -C (47) – C (52) – C (51) – C (50), Cg 12 = C (54) - C (55) - C (56) - C (57) - C (65) - C (66),

Cg 13 = C (58) – C (59) – C (60) – C (61) – C (62) - C (63)

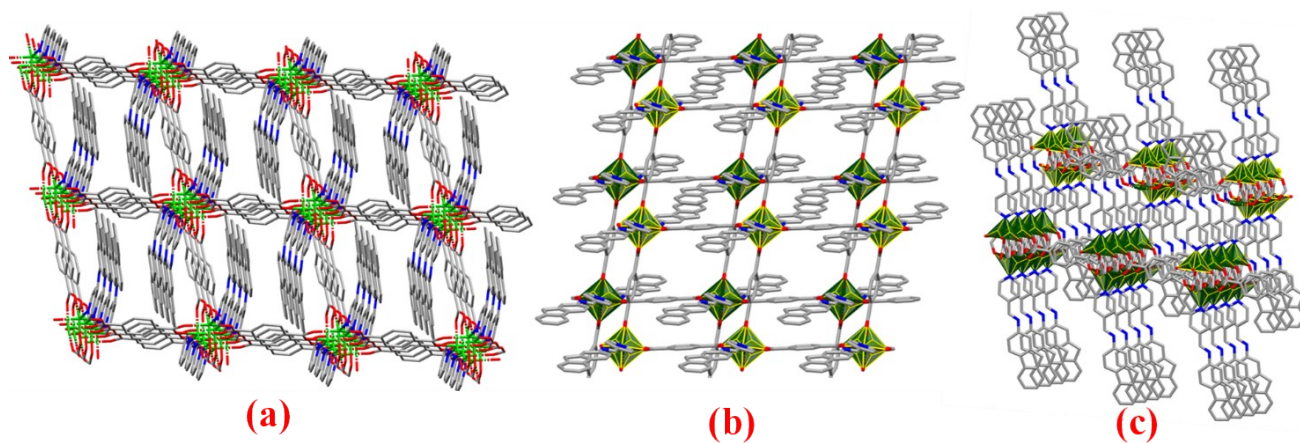| H-bonding interaction				
Donor…H	Acceptor	D - H	H…A	[ARU]
O005--H005A	O1	0.87	2.26	[6555.01]
O00D--H005B	O3	0.87	2.36	[1545.01]

Figure S6. (a) View of supramolecular assemble along an axis; **(b)** Coordination polyhedral around the constituting central metal (Zn) ion, **(c)** Extended supramolecular aggregation of **CP1**.
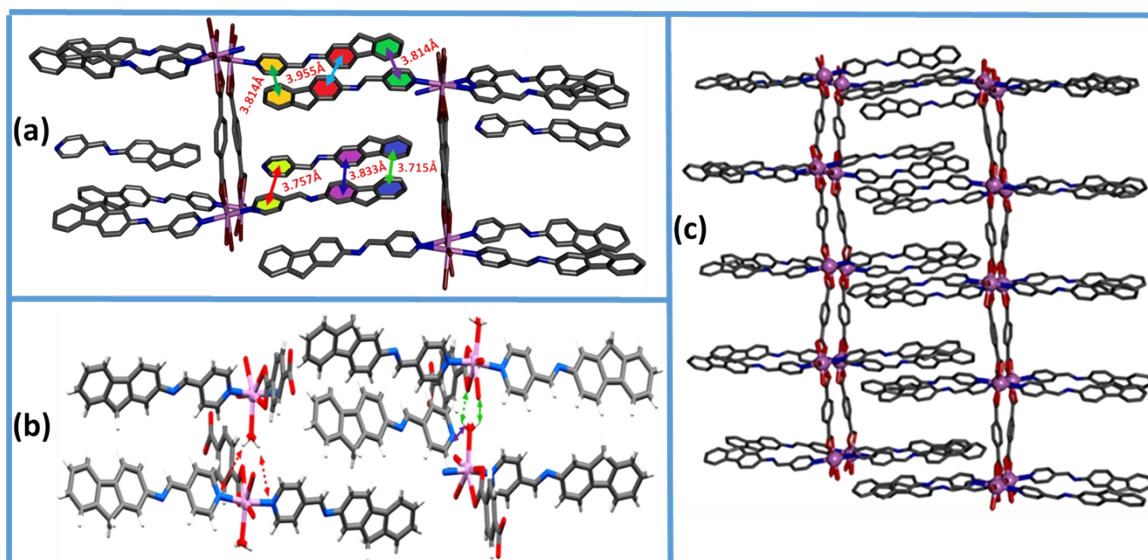

Figure S7. (a) view of the $\pi\cdots\pi$ interaction **(b)** view of H-bonding in different molecular units of **CP2**. (c)View of supramolecular assemble along a axis.
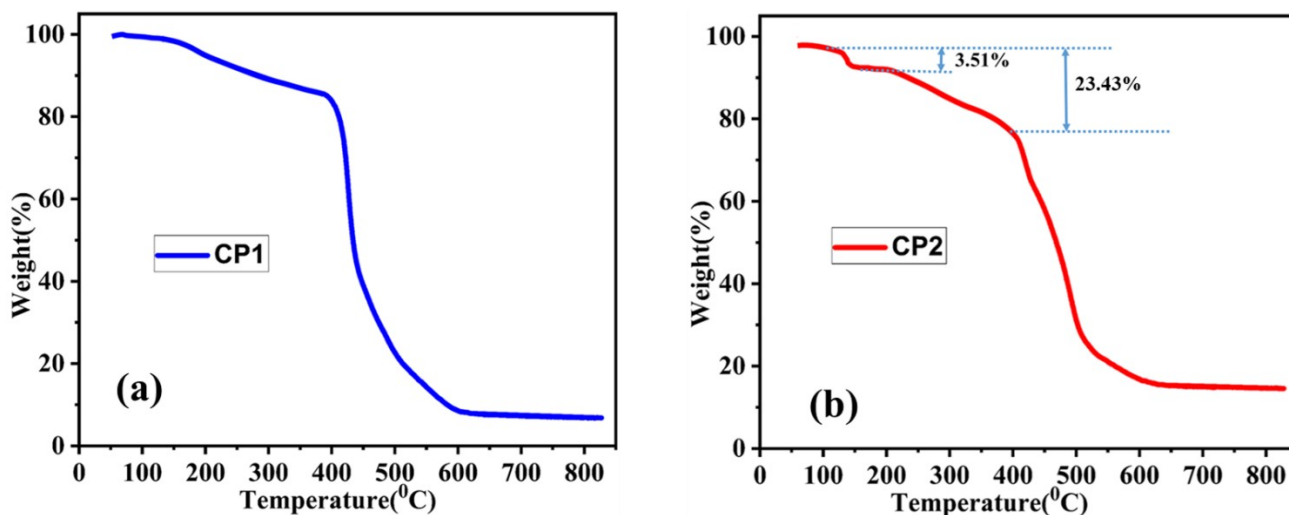
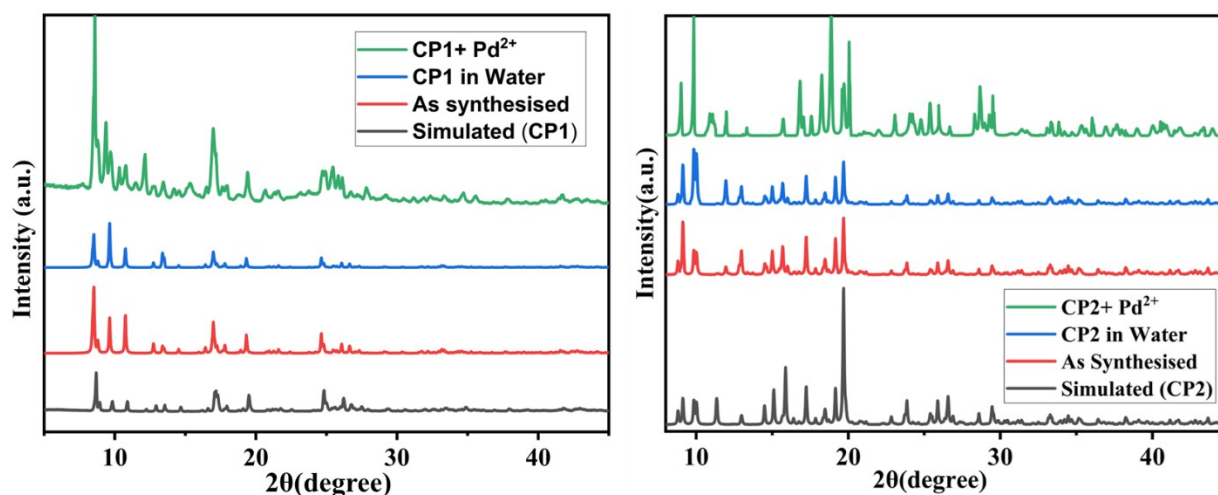**Figure S8.** TGA plots of **CP1(a)** and **CP2(b).**

Figure S9. PXRD patterns of (a) simulated of **CP1** (black); as-synthesize **CP1** (red); **CP1** in water (blue) and **CP1** in presence of Pd^{2+}(green); (b) simulated of **CP2** (black) and as synthesize **CP2** (red); **CP2** in water (blue) and **CP2** in presence of Pd^{2+}(green).

UV-Visible and Fluorescence Spectral Experiments

A suspension of **CP1** (5 mg/10 ml; 1.0×10^{-3} M) and **CP2** (10.5 mg/10 ml, 1.0×10^{-3} M) were prepared in DMF (10 ml) (spectroscopic grade), sonicated for 5 min and the resulting medium was used as stock solution for ion sensing studies. The metal salt solutions (10^{-3} M) of $Zn(NO_3)_2 \cdot 6H_2O$, $CuCl_2.2H_2O$, $NiCl_2.6H_2O$, $CoCl_2.6H_2O$, $FeCl_3 \cdot 6H_2O$, $MnCl_2.4H_2O$, $CrCl_3 \cdot 6H_2O$, $CdCl_2.2H_2O$, $PdCl_2$, $AlCl_3.6H_2O$, $MgCl_2.6H_2O$, $HgCl_2$, $IrCl_3.3H_2O$, $RhCl_3.3H_2O$, $RuCl_3.3H_2O$, $K_2[PtCl_4]$, $CaCl_2.6H_2O$, $BaCl_2.2H_2O$, NaCl, KCl were prepared in MeOH for sensing experiment. The equivalent quantity (25 μM) of metal salt solution was mixed to the diluted stock solution of **CP1/CP2** and pH 7.2 was maintained by adding HEPES buffer in aqueous medium at ambient condition (the resulting

16

solution contains 40 times of water than DMF). UV-Vis **(Figure S10)** and fluorescence spectra **(Figure 3b & 4b)** were collected by adding the salt solution to the solution of CPs for testing sensitivity to the ions. In presence of Pd^{2+}, a blue shift is observed by 14 nm for **CP1** (271 nm) and 8 nm for **CP2** (270 nm) but in presence of other metal ions there have no significant change is observed for both the compounds **(Figure S11)**. The emission intensity was selectively quenched upon addition of aqueous solution of Pd^{2+}only s **(Figure 3a & S12)** while other ions remain insensitive. The Stern-Volmer equation $I_0/I = K_{SV}[Q]+1$ was used to determine the Stern-Volmer constant (K_{SV}), where I_0 and I indicate the emission intensity of **CP1/CP2** in absence of quencher and presence of quencher (Pd^{2+}) respectively and [Q] represents the concentration of quencher. The $3\sigma/M$ method was applied to calculate the LOD (Limit of Detection) value of Pd (II) sensing by **CP1** and **CP2** in aqueous medium where σ and M indicates the standard deviation and slope of calibration curve respectively. Life time plot helps us to evaluate the stability in excited state of coordination polymer. The sensing efficiency of **CP1**/**CP2** were carried out using aqueous suspension of $PdCl_2$.
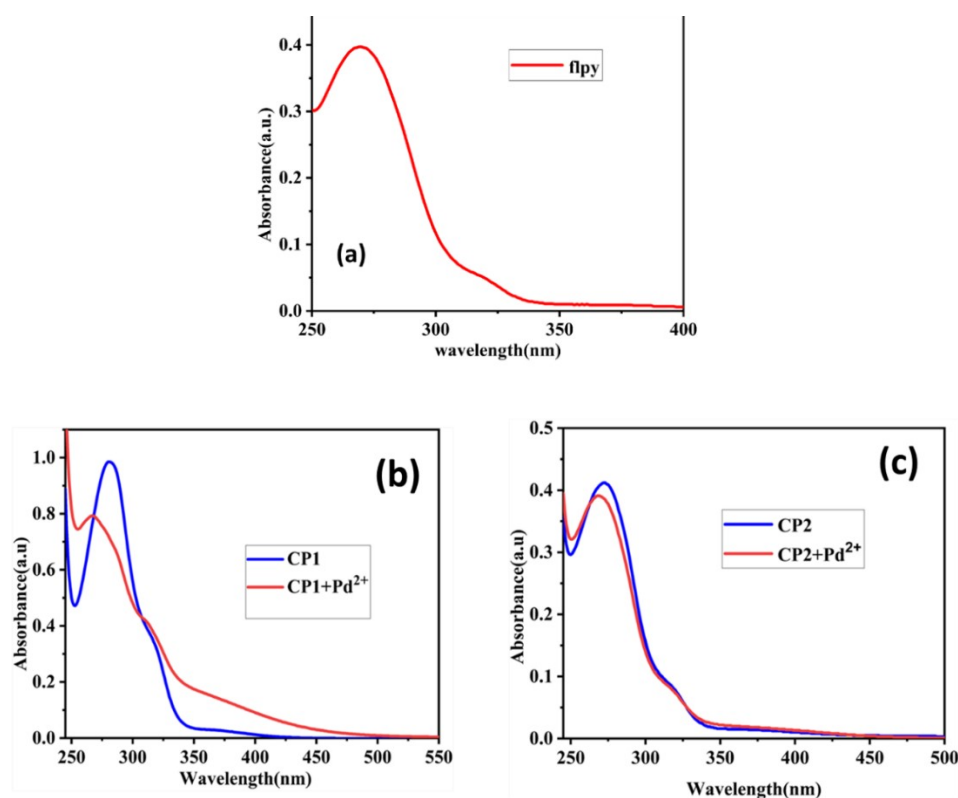

Figure S10. UV-visible spectrum of (a) **flpy** ligand; (b) **CP1** and (c) **CP2** in the absence and presence of Pd^{2+} ion in aqueous medium.
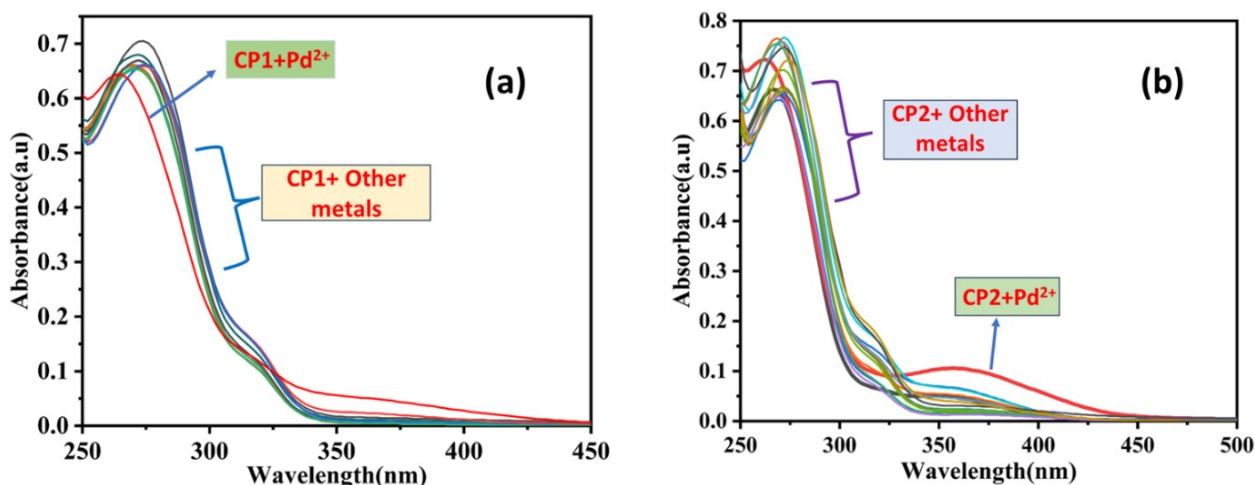
17

Figure S11. Absorption spectra of (a) **CP1** and (b) **CP2** dispersed in aqueous medium in the presence of different metal ions.
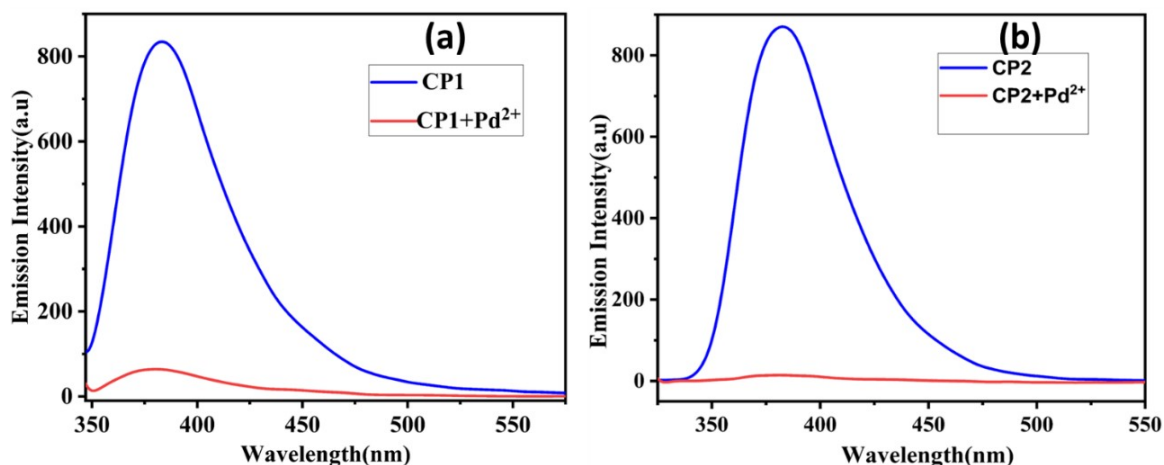

Figure S12. Emission Intensity of (a) **CP1** and (b) **CP2** (c) in absence and presence of Pd^{2+} ion in aqueous medium.

Sensing Experiment and Detection limit calculation of both CPs for Pd(II)

The equivalent quantity (50 mM) of metal salt solution was mixed to the diluted stock solution which was carried out in aqueous medium (HEPES buffer, pH 7.2) at ambient temperature. UV-Vis spectra of the final solution was mentioned former kept in the cuvette provided the excitation wavelength and fluorescence experiments were performed. The Stern-Volmer equation $I_0/I = K_{SV} [Q]+1$ which helps us to determine the Stern-Volmer constant value (K_{SV}), where I_0 and I indicate the emission intensity of CP**1** in absence of quencher and presence of quencher (Pd^{2+}) respectively and [Q] represents the concentration of quencher. The $3\sigma/M$ method is applied to calculate the LOD (Limit of detection)

LOD value of Pd(II) sensing by **CP1** and **CP2** in aqueous medium where σ and M are indicating the standard deviation and slope of calibration curve respectively [Standard Deviation (σ) = 2.14 and 2.25 for **CP1** and **CP2**]. The quenching of emission of CPs by the addition of Pd(II) gradual decrement in emission intensity of the CPs by fluorescence spectroscopic technique. The plot of change in fluorescence intensity versus concentration of Pd(II) revealed a linear curve for **CP1** with a slope (M) of $3.26 \times 10^5\,M^{-1}$ while in case of **CP2** the value was $2.998 \times 10^5\,M^{-1}$ **(Figure S13)**. The ascendent segment of the curve in the plot of (I_O/I) vs Pd^{2+}(μM) signifies specify quenching of the emission of CP1 and CP2 by Pd^{2+}, both static and dynamic, and that the amount of quenching enhances with concentration **(Figure S15).** The limit of detection of Pd(II) for **CP1** and **CP2** in aqueous medium are 0.0791 μM and 0.0892 μM respectively **(Figure S14)** which is comparable with other reported MOF-based sensor materials.[S5-S10]
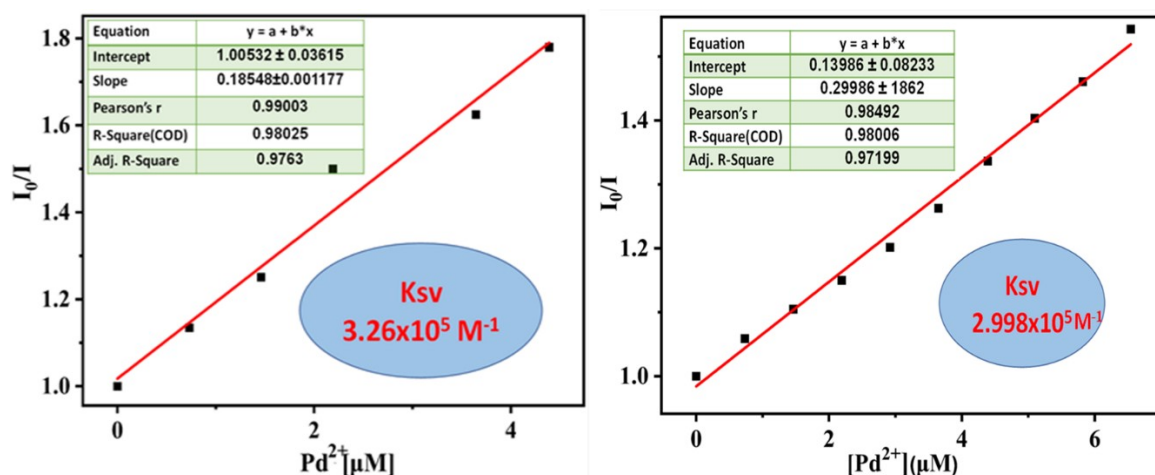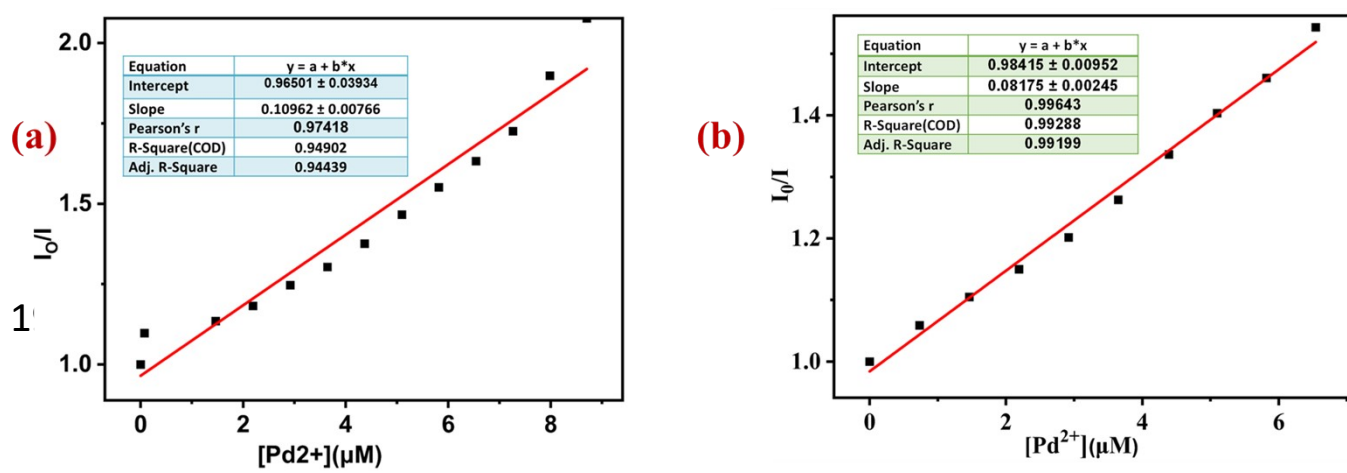

Figure S13. Stern-Volmer plot of **CP1**(a) and **CP2** (b)at lower range of quencher $[Pd^{2+}]$ (in μM) concentration.
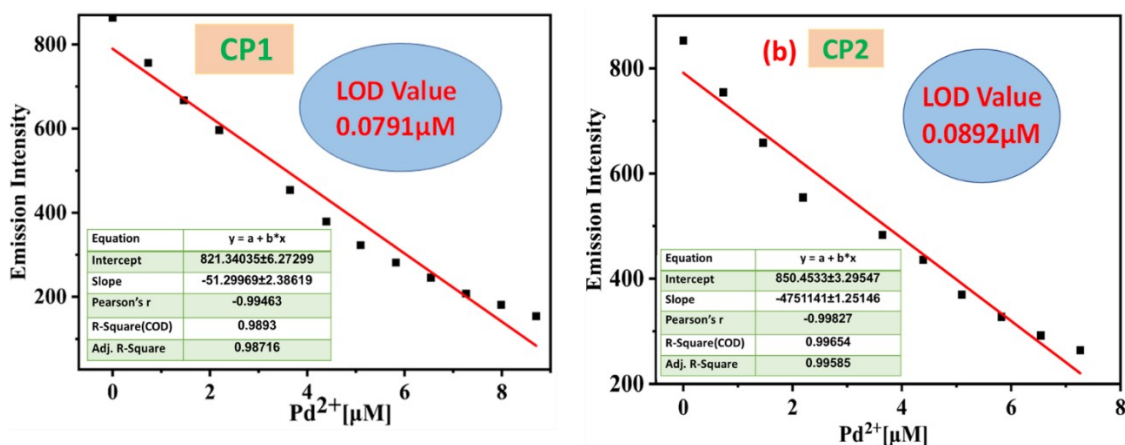
Figure S14. The linear dynamic response of **CP1**(a) and **CP2**(b) for Pd(II) and the determination of the limit of detection (LOD) of Pd(II).
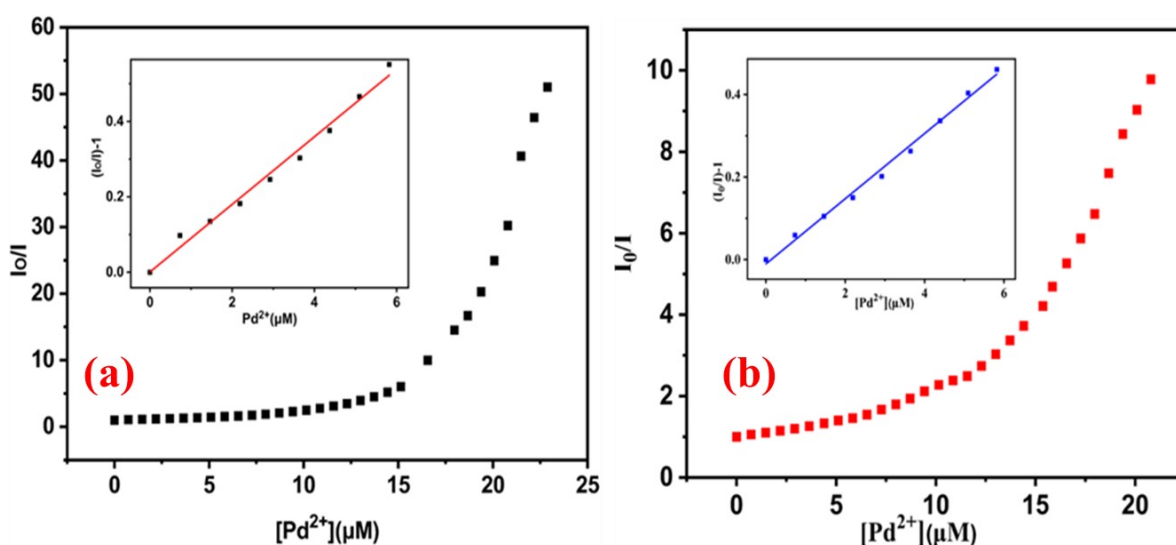

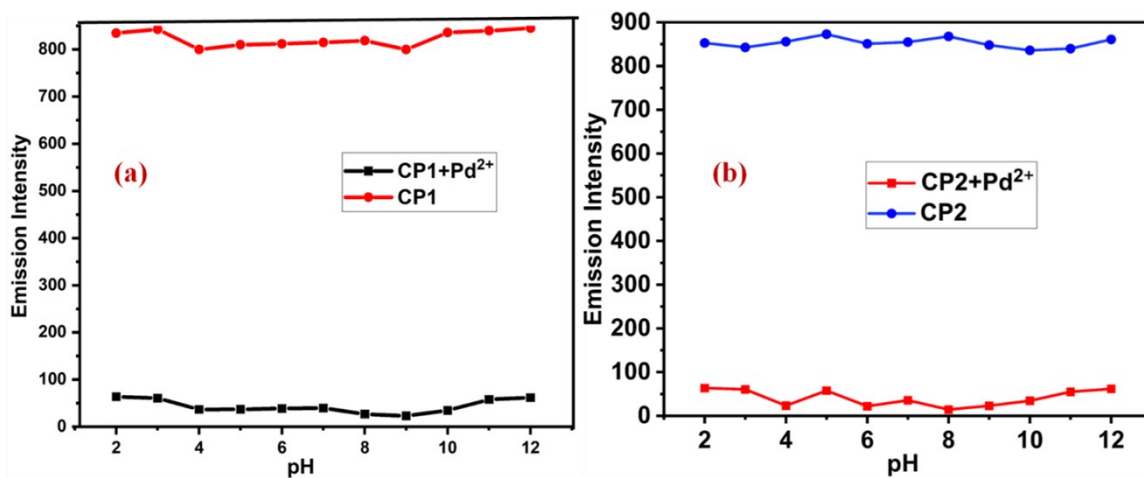**Figure S15.** Stern-Volmer plot of **CP1 & CP2.**

Figure S16. Emission intensity of CP1 and [CP1+Pd^{2+}] **(a)** and CP2 and [CP2+Pd^{2+}] (b) at different pH range (2 to 12)
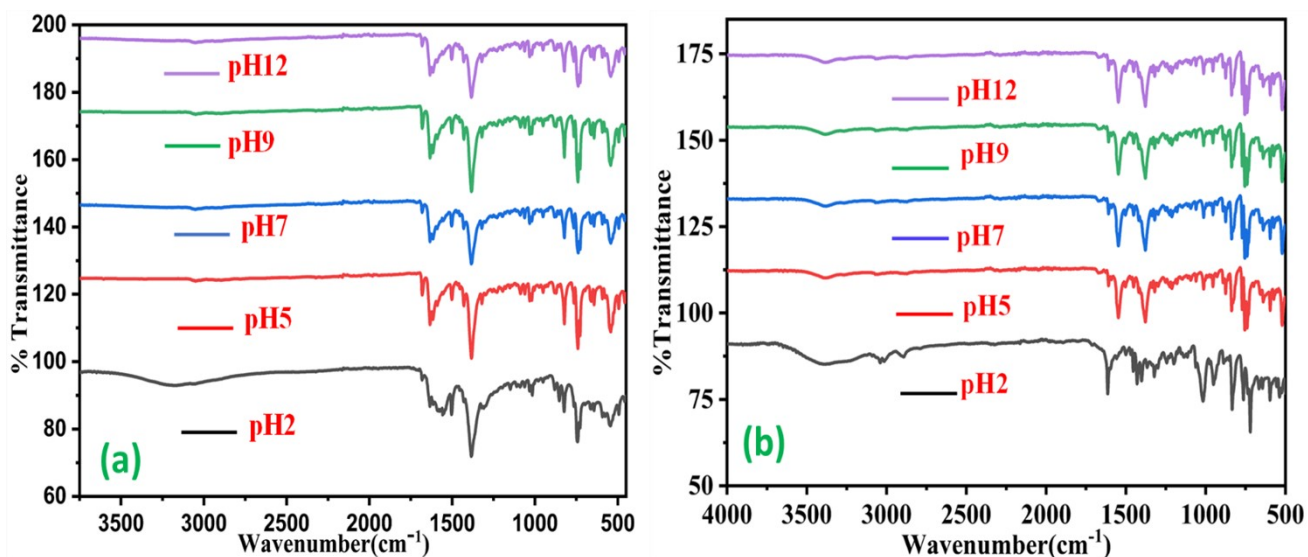
Figure S17. IR spectra of CP**1** (a) and CP**2** (b)at different P^H

(a)

(b)
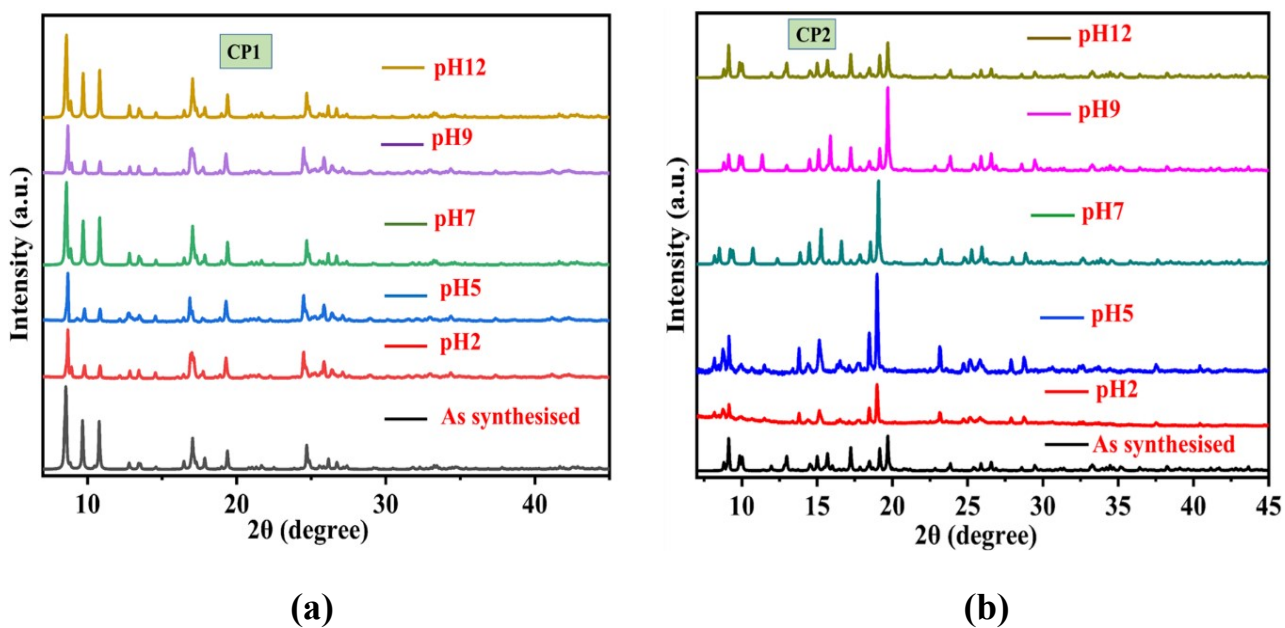
Figure S18. Powder X-ray pattern of (a) **CP1** and (b) **CP2** at different pH.
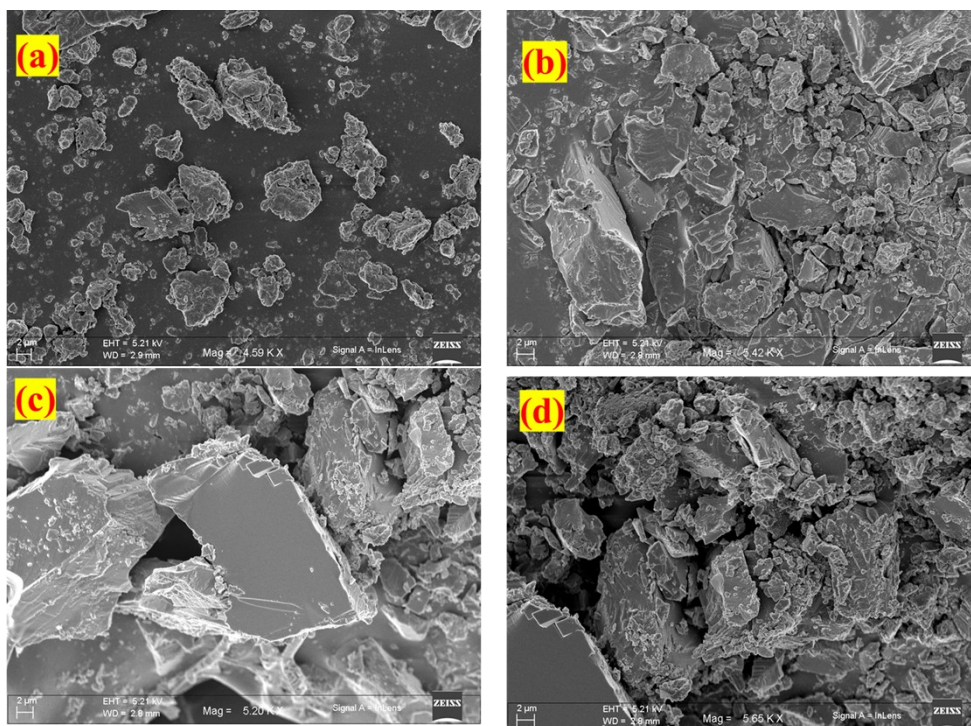
Figure S19. FESEM image of CP**1** at (**a**) pH = 2, (**b**) pH = 4, (**c**) pH = 7 and (**d**) pH =12
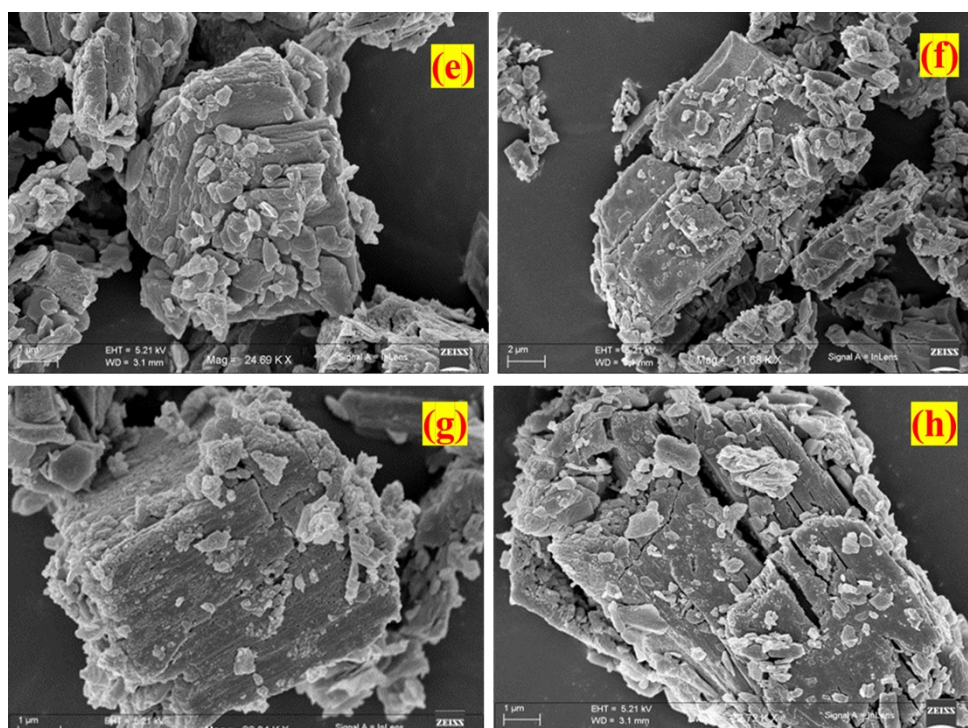
Figure S20. FESEM image of CP**2** at (**e**) pH = 2, (**f**) pH = 4, (**g**) pH = 7 and (**h**) pH =12

Theoretical calculations

To get insights into the binding mode, a theoretical study has been performed. Density functional theory (DFT) were used to the optimized geometry of **CP1** and **CP2** applying the GAUSSIAN-09 software[S11]. All the theoretical calculations were achieved using the hybrid DFT-B3LYP function.[s12] The DFT optimization structures of the **CP1** and **CP2** were evaluated with the LanL2MB and LanL2DZ basic set respectively. The time-dependent density functional theory (TDDFT)[S13-S15] was accomplished to describe all of the distinct low-lying electronic transitions in the spectra. The Gauss sum[S16] calculation was used to evaluate the fractional entanglement of the polymeric compounds for every molecular orbital. Use of full polymeric network in the DFT computation is not formidable, and only coordination repeating motif is considered for the calculation.

Table S7. DFT table of both the compounds.

Compounds Name	Exp. Wavelength (nm)	Theo. Wavelength (nm)	Energy (eV)	Frequency	Transition
Ligand(flpy)	264	261.65	4.7386	0.0267	HOMO-5→ LUMO (36.21 %)
CP1	320	319.69	3.9266	0.1231	HOMO→ LUMO +5 (40.18 %)
CP2	314.93	314.48	3.9425	0.0002	HOMO-8→LUMO (49.4%)
CP2	277.86	277.85	4.4622	0.2193	HOMO-23→LUMO (44%)

23
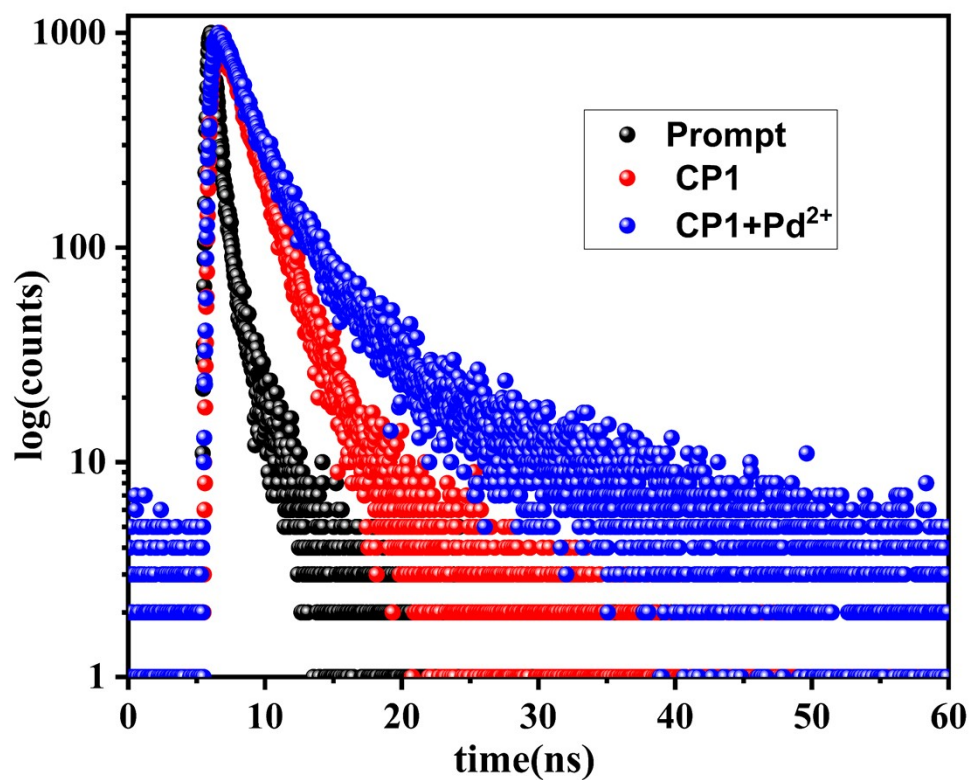
Figure S21. Excited state stability of **CP1** and [**CP1+Pd²⁺**]
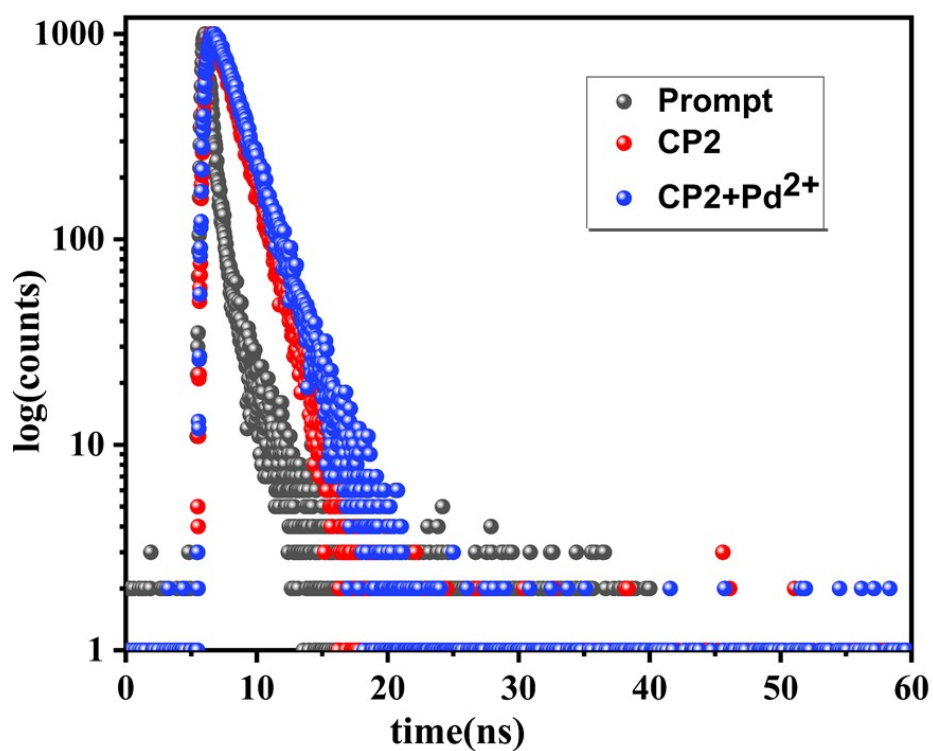
Figure S22. Excited state stability of **CP2** and [**CP2+Pd²⁺**]
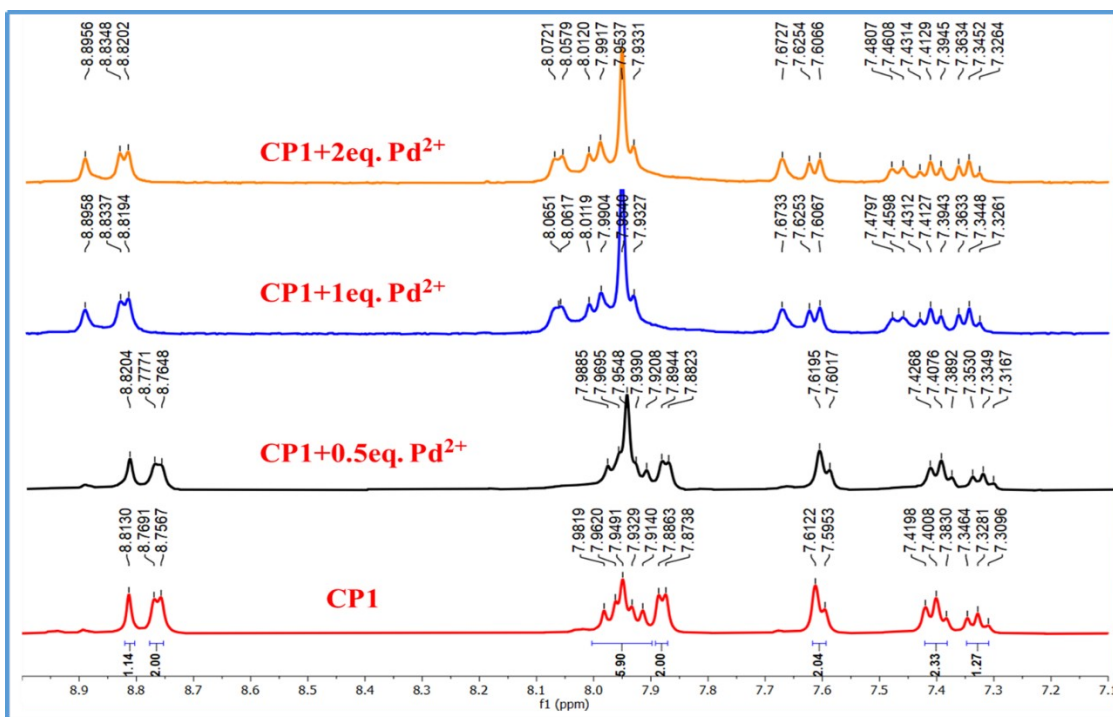
Figure S23. ^{1}HNMR (400 MHz, DMSO-d$_6$) spectra of **CP1** and **CP1+ Pd^{2+}.**
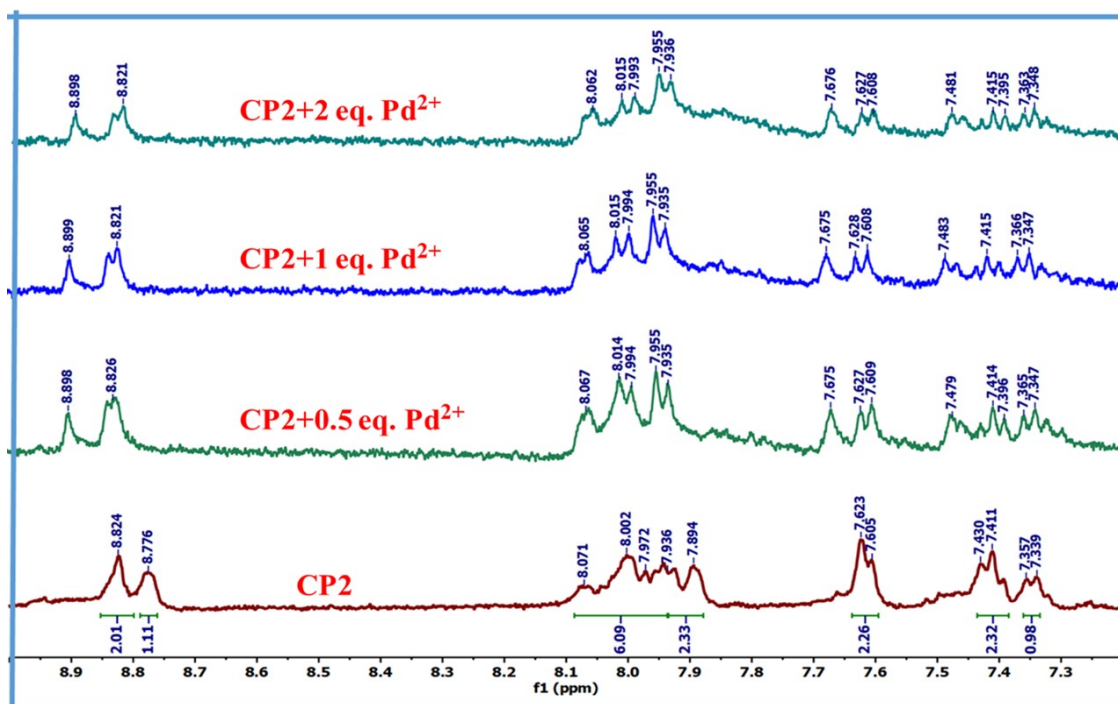
Figure S24. ^{1}HNMR (400 MHz, DMSO-d$_6$) spectra of **CP2** and **CP2+ Pd^{2+}.**

Table S8. Comparison of the sensitivities of **CP1** and **CP2** with previously reported CPs to detect Pd^{2+} ion.

Sl. No	Ligand	Selectivity (LOD)	Solvent	Reference
1	**[Cd(4-nvp)2(5-ssa)]** [4-nvp = 4-(1-naphthylvinyl) pyridine and 5-ssa = 5-sulfosalicylic acid]	0.09 µM	Water	17.
2.	**[Tb(ppda)(npdc)0.5(H₂O)₂]n** 4-(pyridin-3-yloxy)-phthalic acid (H2ppda) and1,4naphthalenedicarboxylic acid(H₂nbdc)	94.4 µM.	Water	18.
3.	**[Zn₂(1,2,3,4-tcpb)4(bpeb)₂]** (bpeb=1,4-bis[2-(4-pyridyl)ethenyl]benzene), (H₄tcpb = 1,2,4,5-tetrakis(4-carboxyphenyl)benzene)	0.03 µM	DMF	19.
4.	**{[Zn(fum)(4-nvp)2]·2H2O}n (1)** **{[Zn(mes)(4-nvp)2]·H2O}n (2)** **[Zn(glu)(4-nvp)]n (3)** (H₂fum =fumaric acid, 4-nvp = 4-(1-naphthylvinyl)pyridine, H₂mes = mesaconic acid and H₂glu-glutaric acid)	0.132 µM (**1**) 0.146 µM(**2**) 0.152 µM (**3**)	Water	20.
5.	**[Cd(AIPA)(tppz)(H₂O)]n** (tppz = 2,3,5,6-Tetrakis(2-pyridyl)pyrazine, AIPA = 5-	0.08 µM	Water	21.

	Aminoisophthalic acid)			
6.	[Al(OH)(IPA-OC3H3)] ·0.5H2O·0.05DMF (H2PIA =5-(prop-2-yn-1-yloxy)isophthalic acid)	102 nM	water	22
7.	$[Zn_2(bdc)_4(flpy)_2]_n$ (CP1) $[Cd(bdc)_2(flpy)_2(H_2O)]_n \cdot (flpy)$ (CP2) Flpy=9H-Fluoren-2-yl-pyridin-4-ylmethylene-amine H_2bdc =1,4-benzenedicarboxylic acid	0.0791 μM (CP1) 0.0892 μM (CP2) (Pd^{2+})	water	This work

N. B.: Every Reference of the Table S8 is included in the main manuscript.

The literature survey of Pd^{2+} sensing by Coordination Polymers (CPs) as transducer (**Table 8)** shows the sensitivity of **CP/MOF** to Pd^{2+} ions with LOD value. The sensing efficacy of **CP1** and **CP2** to Pd^{2+} in aqueous solution shows the second lowest LOD value that makes both the compounds very impactful.

Chakraborty et al. reported that[22] new ultrasensitive and ultrafast Al(III) based MOF (**1**) was constructed to detect Pd^{2+} ions. The quenching in the fluorescence signal was observed due to the weak interaction between the linker alkyne−π bond and Pd^{2+} having LOD 102 nM. Dutta et al. also utilised Cd based CP to detect Pd^{2+} in which in which Pd^{2+} is encapsulated between two naphthyl ring having LOD value 0.09 μM.[17] Our group also reported that Pd^{2+} may be a coordinate bond to carboxylate−O of free −COOH in **CP1** and be placed in the interlayer.[21] There is sufficient space between the two oxygen atoms of two layers along with sufficient π⋯π distance and Pd^{2+} may be accommodated there in without any steric hindrance having LOD 0.08 μM.

In this work, the fluorogenic motif of both CPs are same, **flpy**, but there has some structural difference between two frameworks – Zn(II)-CP is 2D CP and Cd(II)-CP is 1D CP. The 2D paddle-wheel like structure of **CP1** has higher tendency to interact with Pd^{2+} than the 1D fish bone like skeleton of **CP2**. Therefore, the careful investigation of the results indicate that CPs selectively and specifically accommodate Pd^{2+} only in the framework through the coordination of the imine-N (-C=N-) of the SBU unit and stabilising by the inclusion in the π-cavity of fluorenyl moiety of the pendant Schiff

base. This association may encourage energy transfer from excited [CPs]* to the Pd^{2+} and quenches the emission. Consequently, the Stern–Volmer constant (K_{SV}) of Pd^{2+}(aq) for **CP1** (3.26×10^5 M^{-1}) is higher than **CP2** (2.998×10^5 M^{-1}). The limit of detection of Pd^{2+}(aq) for **CP1** (0.0791 µM) is slightly better than **CP2** (0.0892 µM). Therefore, **CP1** has higher sensing ability than **CP2** towards Pd^{2+}.
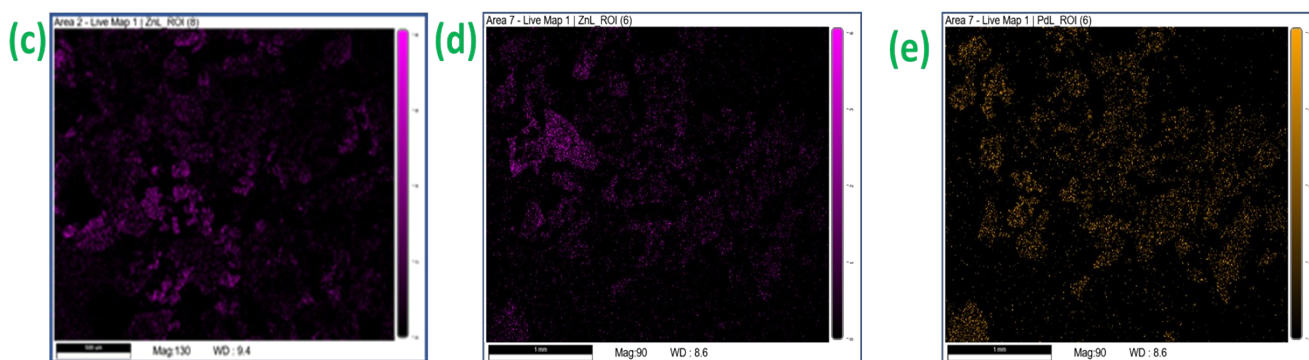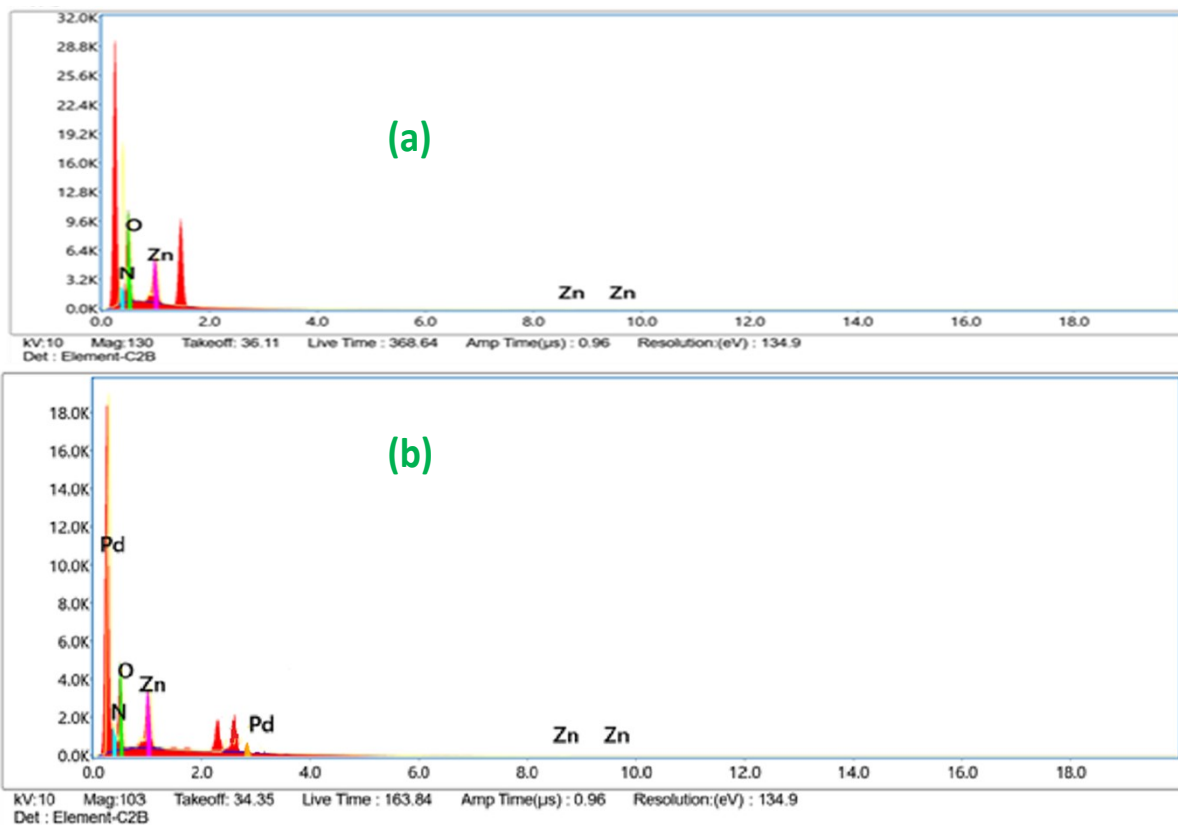

Figure S25. EDS spectra of CP**1**(a)**;** [CP**1**+Pd^{2+}] (b)**;** Mapping of Zn in CP**1** **(c);** SEM EDS mapping of Zn in CP**1** in addition of Pd(II); **(d)** Mapping of Pd in CP**1** in addition of Pd(II) **(e).**

28
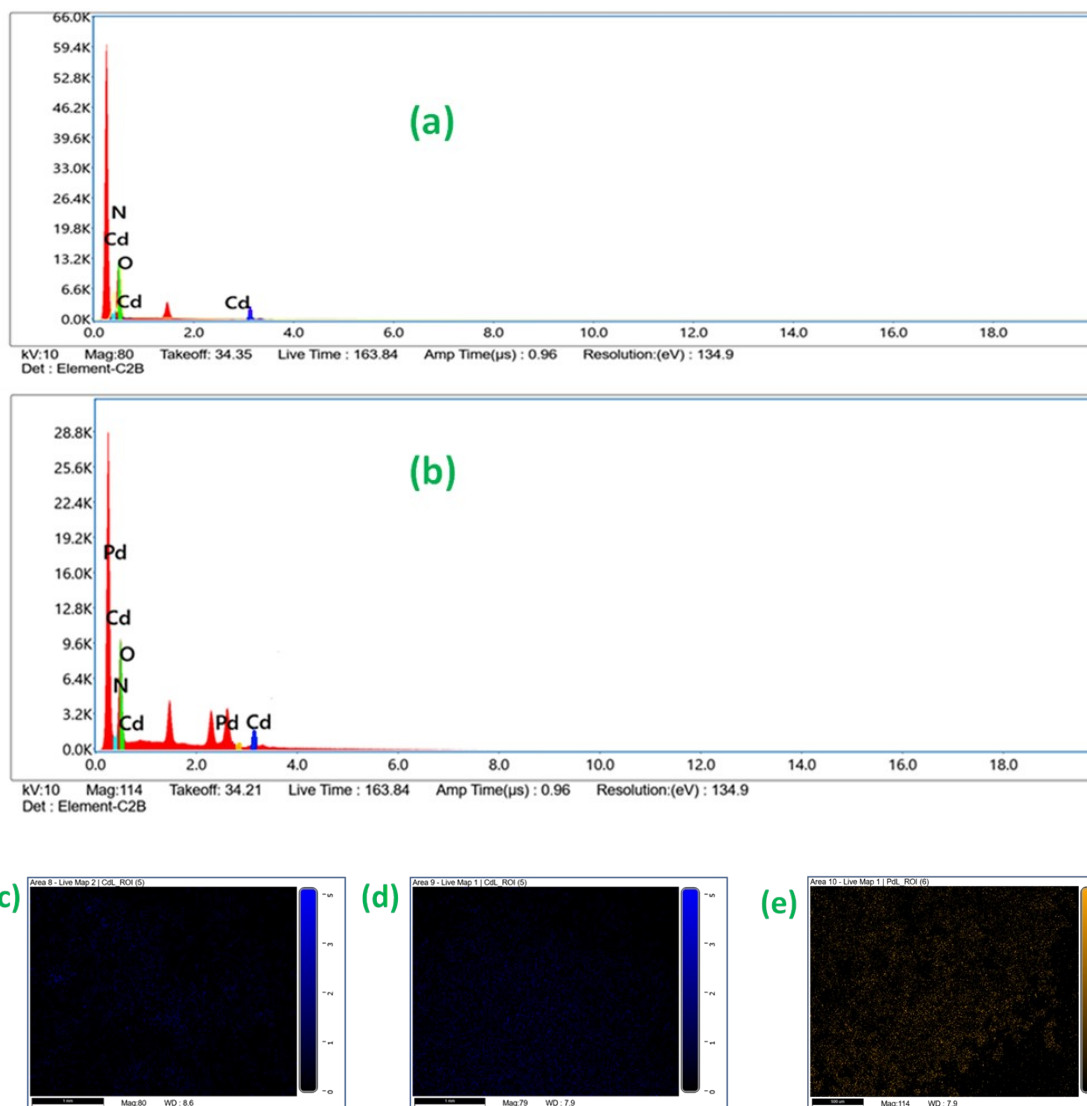
Figure S26. EDS spectra of CP**2**(a)**;** [CP**2**+Pd^{2+}](b) ;Mapping of Cd in CP**2** **(c);** SEM EDS mapping of Cd in CP**2** in addition of Pd(II); **(d)** Mapping of Pd in CP**2** in addition of Pd(II) **(e).**

Table S9. Atomic % of the CP**1** and [CP**1**+Pd^{2+}]

Sample	Metal of CPs (%)	O%	N%	Pd%
CP1	7.40	38.40	54.20	-
[CP1+Pd^{2+}]	7.20	35.50	56.8	0.50
CP2	9.92	73.79	16.29	-
[CP2+Pd^{2+}]	8.12	75.38	15.95	0.55

Figure S27. XPS spectrum of Pd $3d_{5/2}$, $3d_{3/2}$ for the in presence of $PdCl_2$ in **CP**s.
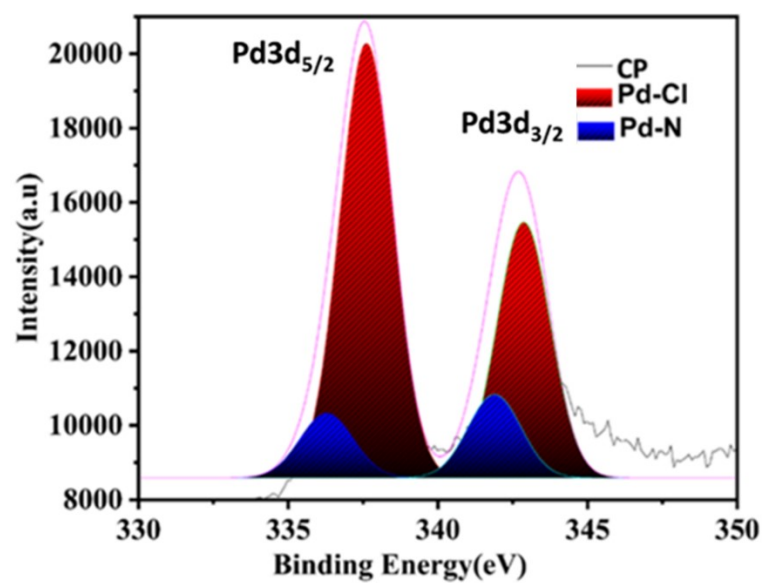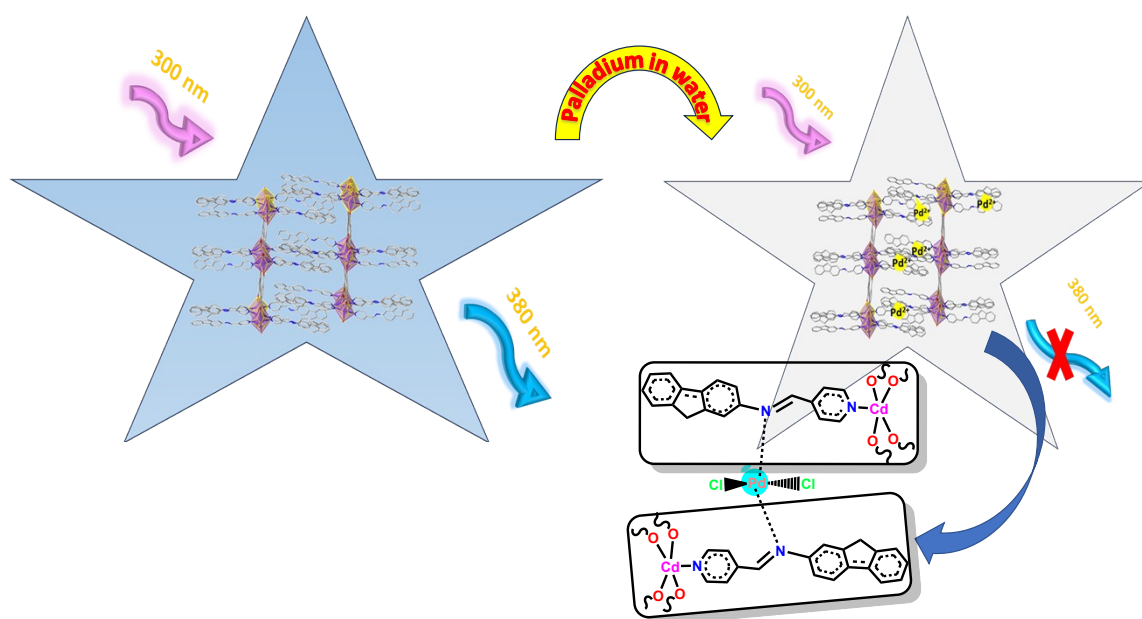

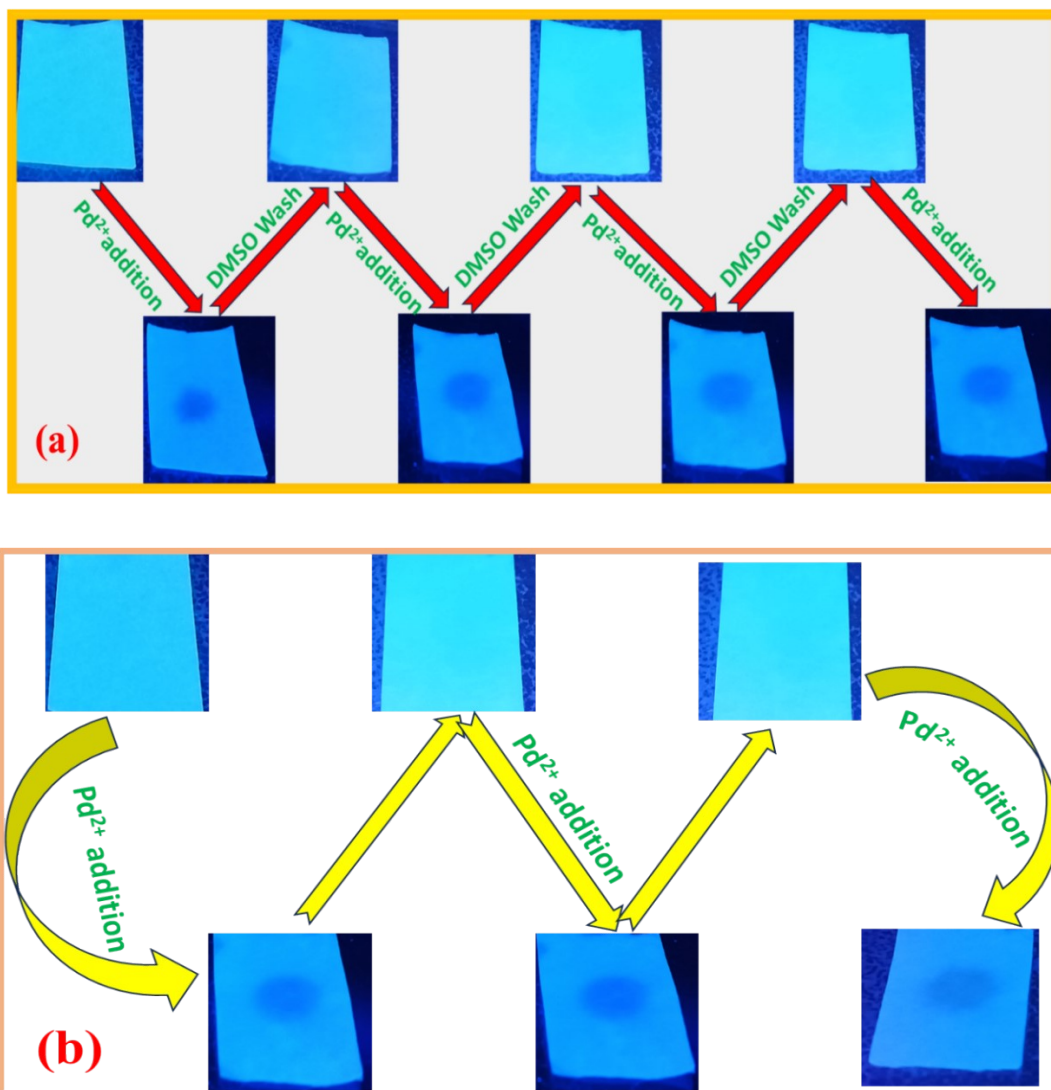**Figure S28.** Possible mechanism of the fluorometric "turn-off" sensing of Pd^{2+} by the **CP2** in aqueous medium.

Figure S29. Paper strip experiment for recyclability of (a) **CP1** & (b) **CP2** towards Pd^{2+}.

Fabrication and Characterization of the device

Two different synthesized materials are used in the fabrication of thin film semiconducting devices to examine their electrical properties. In this context, synthesised materials are used to create Schottky diodes, and device characteristics are examined. Indium Tin Oxide (ITO)-coated glass substrates are cleaned with acetone, ethanol, and distilled water consecutively employing ultrasonication technique before the manufacturing of devices. The substrates are then dried in a N_2 environment at ambient temperature. Homogeneous dispersions of synthesized materials in N, N dimethyl formamide (DMF) medium (2mg/mL) are obtained using ultrasonication. Later, using a spin coater, two dispersions are

coated on two distinct ITO-covered glass substrates to produce thin films. The systems are vacuum-dried after that. A surface profiler is used to measure the films' thickness which is nearest to one
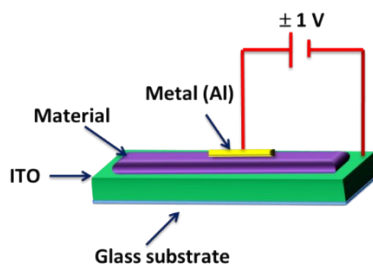
Figure S30. Schematic representation of Schottky diodes.

micrometre. Then, using a vacuum coating unit aluminium (Al) metal is coated onto the films at a pressure of 10^{-6} Torr. In the time of aluminium coating a shadow mask is used to keep the effective areas as 7.065 10^{-6} m^2. By recording current-voltage (I-V) data from a Keithley 2635B source meter (using a two-probe method) characterization of the electrical properties of the devices are done. All preparations and characterizations are done at room temperature (303K).

Figure S31. (a) XPS in the valence band region of the **CP1**. (b) Tauc plot to determine the optical band gap of the **CP1**.

Figure S32. (a) XPS in the valence band region of the **CP2**. (b) Tauc plot to determine the optical band gap of the **CP2**.

32

Figure S33. Band diagram of **CP1 (a)** and **CP2(b)** from **Figure S30** and **Figure S31**.
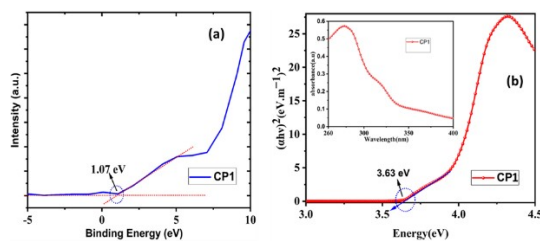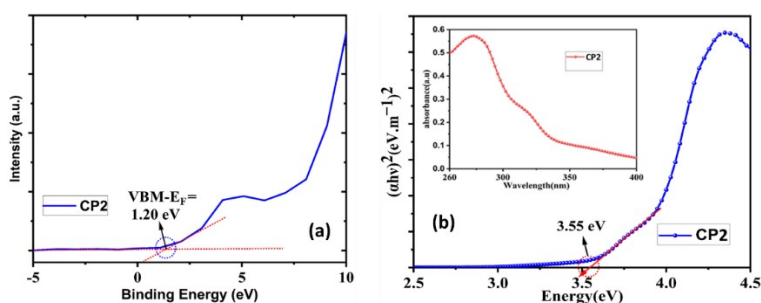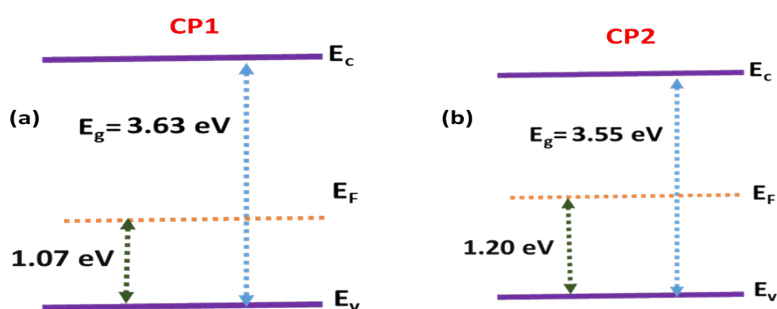
Comparison of the electrical conductivity properties of CP1 and CP2 with previously reported CPs

Literature survey is summarised in the **Table S10.** However, the reported compounds (**CP1** and **CP2**) revealed that some of them enhanced conductivity upon device fabrication but most of them are not performed well with respect our compounds; in view of chemical, physical, thermal stability of our compounds may be appropriate candidate towards future generation technical advancement.

In the regard, Mandal et al. synthesised a series of Cd based coordination polymer[S23] with variety of ligands. They revealed that the conductivity of the device has been generated for highly delocalized π-electrons of organic ligands act as electron donors and pseudohalide-based Cd(II) metal parts (inorganic parts) serve as the electron acceptor during photo excitation. Here, conductance increase in the order **4 > 2 > 3 > 1** that explained by distinguishable coordination environments around the Cd(II) centre. In **1** and **3**, having 1D chains while 3D structure of **2** and **4** are found. They have been shown a significant change in the donor–acceptor character has been found due to accumulation of more inorganic parts [Cd(II) metal-based pseudohalide parts] within the 3D architecture of CPs **4** and **2** probably plays a crucial role in increasing charge transportation, resulting in high conductance values. Again, Saha et al. reported that[S25] two MOFs (**Co-MOF**, **Ni-MOF**) by helping a flexible bispyrazole based ligand and 2-sulphono terephthalic acid to fabricate electrical devices by utilizing the immobilized free sulfonic groups and encapsulated H-bonded water clusters for active charge species generation and transportation through-space, adopting a so-called "hopping" mechanism. These kinds of noncovalent interaction-mediated charge transportations often turned out to be the main driving force of optoelectronic device fabrication.

Table S10. Comparison of the electrical conductivity

Sl. No	Compound	Dimension	conductivity σ(Sm^{-1})	References
1	[Cd(**L1**)(NCS)$_2$·H$_2$O]$_n$ (**1**)	1D	1.37 × 10^{-5} (D) 5.06 × 10^{-5}(L)	S23
	Cd$_{1.5}$(L1)(N(CN)$_2$)$_3$]$_n$ (2)	3D	1.85 × 10^{-5}(D) 8.78 × 10^{-5}(L)	
	[Cd(**L2**)(NCS)$_2$]$_n$ (**3**)	1D	1.61 × 10^{-5}(D) 7.26 × 10^{-5}(L)	
	[Cd$_{1.5}$(L2)(N(CN)$_2$)$_3$]$_n$ (4) (Where, L1, L2, L3, L4 = Chromone-based Schiff base)	3D	2.01 × 10^{-5}(D) 10.21×10^{-5}(L)	
2.	[Cd (glu)$_2$ (pbiq)$_2$ (H$_2$O)]$_n$ (pdiq = pyridyl-imidazoquinazoline; H2tdc = 2,5-thiophenedicarboxylic acid	1D	1.10 × 10^{-5} (D)	S24
3.	{[Co$_{1.5}$(STA)(H$_2$MDP)(H$_2$O)$_3$]·3H$_2$O}$_n$	3D	9.09 × 10^{-5} (D) 6.31 × 10^{-4} (L)	S25
	[Ni$_2$(STA)$_2$(H$_2$MDP)$_2$(H$_2$O)$_4$]$_n$ (where H$_2$STA = 2-sulfono terephthalic acid, H$_2$MDP= methylenebis(3,5-dimethylpyrazole)	3D	1.80 × 10^{-4}(D)	
4.	Cd (tppz) (adc) (MeOH) (1) (where tppz= 2,3,5,6-tetrakis(2-pyridyl)pyrazine) , H2adc = acetylene dicarboxylic acid	2D	5.06×10^{-5}(L), 4.72×10^{-5}(D)	S26
	[Cd(tppz)(trep)] (2) (H2trep = terephthalic acid)	2D	1.80×10^{-4} (L) 1.10×10^{-4} (D)	
	[Cd(tppz)(2,6-ndc)] (3) 2,6 H$_2$ndc = 2,6-naphthalene dicarboxylic acid.	1D	1.93×10^{-3} (L), 1.12×10^{-4} (D)	
5.	[Cd(AIPA)(tppz)(H$_2$O)]n (tppz = 2,3,5,6-Tetrakis(2-pyridyl)pyrazine, AIPA = 5-Aminoisophthalic acid)	2D	7.42×10^{-5} (D) 1.45×10^{-4} (L)	S21
6.	[Zn$_2$(BDC)$_4$(QPR)$_2$(H$_2$O)]$_n$ (BDC^{2-} =1,4benzenedicarboxylato; QPR = 7-[(pyridin-4-ylmethylene)-amino]-chromen-2-one)	2D	8.07 × 10^{-3} (D) 9.26 × 10^{-3} (L)	S27
7.	[Zn$_2$(4-spy)$_2$(bdc)$_2$]$_n$ (1) [4-spy = 4-styrylpyridine]	2D	4.39 × 10^{-4}	S28
8.	[Cu(5-nip)(3-Clpy)$_2$]$_n$ (1) 3-Clpy= 3-chloropyridine	1D	1.58 × 10^{-3}	S29
	[Cu(5-nip)(3-Brpy)$_2$]$_n$ (2) (H$_2$5-nip = 5-nitroisophthalic acid, 3-Brpy=3-bromopyridine.	1D	7.25 × 10^{-4}	
9.	[Ni(L1)(NCS)$_2$]$_n$ (1)	1D	7.0 × 10^{-5} (D) 3.5 × 10^{-4} (L)	S30
	[Ni(L2)(NCS)$_2$]$_n$ (2). (L1 and L2= 8-Aminoquinoline-based Schiff base ligands)	1D	2.0 × 10^{-5} (D) 4.9 × 10^{-4} (L)	
10.	[Cd(quin)$_2$(4-nvp)$_2$] (1); (Hquin = quinoline-2-carboxylic acid and 4-nvp = 4-(1-naphthylvinyl)pyridine)	1D	7.36 × 10-5	S31
	[Cd(quin)$_2$(*rctt*-4-pncb)]$_n$ (1′); (*rctt*-4-pncb = 1,3-bis(4′-pyridyl)-2,4-bis(naphthyl)cyclobutane)	1D	8.84 × 10-6	
11.	{[Zn(H$_2$MBP)$_{1.5}$](BF$_4$)}$_n$ (1)	1D	8.71 × 10^{-5}	S32
	{[Zn$_3$(H$_2$MBP)$_4$(H$_2$O)$_4$(SO$_4$)$_3$](H$_2$O)$_7$}$_n$ (2) 4,4′-Methylene-bispyrazole (H$_2$MBP)	3D	5.79 × 10^{-4}	
12.	[Cu(nip)(4-phpy)$_2$]$_n$ (1) (H$_2$nip = 5-nitroisophthalic acid and 4-phpy = 4-phenylpyridine)	1D	7.56 × 10^{-6}	S33

No.	Compound	Dim.	Conductivity	Ref.
13.	$[Zn_6(bpd)_3(p\text{-}clba)_6(\mu3\text{-}OH)_4]\cdot(p\text{-}clba)_2\cdot(CH_3OH)$, (1)	1D	3.29×10^{-4}	S34
	$[Zn_6(bpd)_3(p\text{-}brba)_6(\mu3\text{-}OH)_4]\cdot (p\text{-}brba)_2\cdot(CH3OH)$, (2) (bpd = 1,4-bis(4-pyridyl)-2,3-diaza-1,3-butadiene, H2p-clba = para-chlorobenzoic acid and H2p-brba = para-bromobenzoic acid)	1D	2.22×10^{-4}	
14	$[Cd_2(2,2'\text{-}DSB)_2(INH)_2(H_2O)_2]_n$ (1) 2-mercaptobenzoic acid (2-MBAH), and isoniazid (INH).	2D	1.05×10^{-3} (D) 2.34×10^{-3} (L)	S35
15.	$[Zn_2(bdc)_4(flpy)_2]_n$ (CP1)	2D	1.285×10^{-4}	
	$[Cd(bdc)_2(flpy)_2(H_2O)]_n.(flpy)$ (CP2) Flpy=9H-Fluoren-2-yl-pyridin-4-ylmethylene-amine H2bdc =1,4-benzenedicarboxylic acid	1D	2.399×10^{-4}	This work

L=light, **D**= Dark

Our group reported three pyrazine based Cd(II) CPs (1−3)[S23] three different dicarboxylates as a bridging ligands. The structural motifs are assembled via $\pi\cdots\pi$- and H bonding and exhibit appreciably high electrical conductivity and have been improved by light irradiation. For higher conjugation, the band gap decreases that explained the ordering (**3**> **2** > **1**) of the electrical conductivity measured from the optical devices fabricated that also supported by the surface morphology by FESEM micrographs of the compounds having higher surface area and were conveyed to a higher contact area and resulted in efficient charge transportation as well as higher electrical conduction. The organic ligands act as antennae of the polymeric chains to collect light energy. Therefore, during the illumination, these ligands absorb light and boost the charge carriers, resulting in an upsurge in mobility and improvement of electrical conductivity. As a consequence of this, this naphthalene-based system has been highly efficient in the above activity and exhibited higher conductivity. In addition, distance within polymeric layers and secondary interactions plays a pivotal role in the exhibition of electrical properties.[S26]

On the other hand, Dutta et al. exposed the Most of the photochemical [2 + 2] cycloaddition reactions [31] have been carried out using UV radiation and shows the impactful effect the conductivity. They synthesised $[Cd(quin)_2(4\text{-}nvp)_2]$ (**1**) which undergoes sunlight-induced [2 + 2] cycloaddition and get dimerized product $[Cd(quin)_2(rctt\text{-}4\text{-}pncb)]_n$ (**1'**) ; confirms by SCXRD. Because of this structural change, the conductivity of **1** depicts approximately ~9 times better than **1'**. It should be mentioned that the presence of $\pi\cdots\pi$ interactions among the aromatic rings of the quin ligands in compound **1** results an increase in charge transport and, consequently, enhanced conductivity. On the other hand, because of the disappearance of $\pi\cdots\pi$-stacking interactions in **1'**, the charge-carrier mobility significantly decreases.

In this work, the presence of more delocalized 4d function in Cd(II), the H-bonding interaction in **CP2** and the $\pi\text{-}\text{-}\text{-}\pi$ interaction between the layers of coordination frameworks with encapsulated delocalised free **flpy**. These non-covalent interactions certainly assist for easier charge

communication than binuclear Zn(II) (3d) synthon in **CP1**. Again, FESEM picture tells the surface morphology of the compounds which provide the shape of **CP1** and **CP2** are block and rectangular respectively. Rectangular shaped has higher contact area and resulted efficient charge transportation as well as higher electrical conduction. For this reason both the materials show higher and efficient electrical conductivity than many other materials.
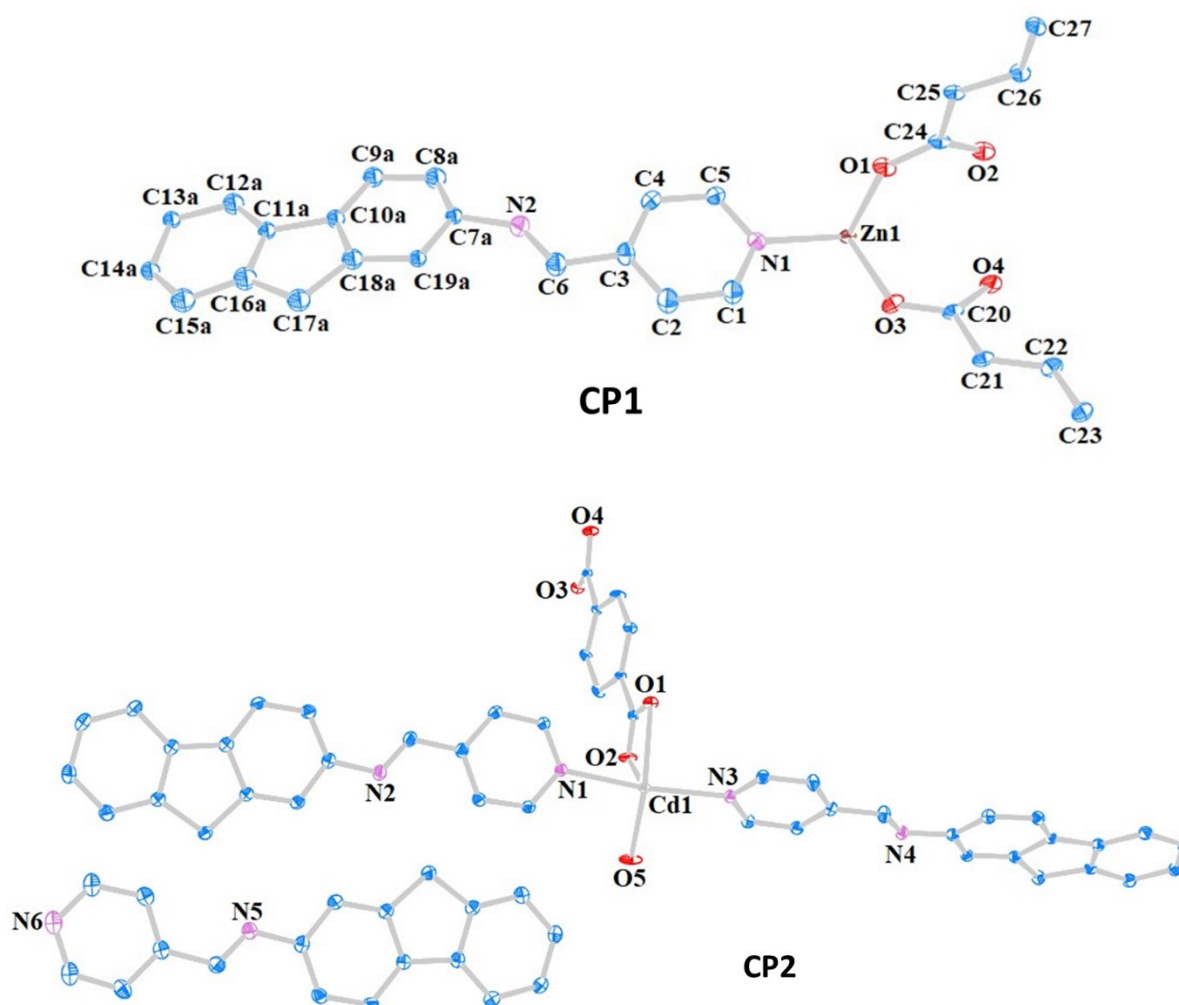

Figure S34. The ORTEP diagram of **CP1** and **CP2**.

References

(S1) G. M. Sheldrick, SADABS, Ver. 2.03; Bruker AXS. Inc.: Madison, WI. 2000.

(S2) G. M. Sheldrick, SADABS: Software for Empirical Absorption Correction, University of Gottingen. 1999. Institute fur Anorganische Chemieder universitat, Gottingen, Germany (1999–2003).

(S3) G. M. Sheldrick, Program for the refinement of crystal structures. SHELXL-93. 1993.

(S4) G. M. Sheldrick, *Acta Crystallogr. C Struct. Chem.,* 2015, **71**, 3-8.

(S5) A.K. Bhanja, S. Mishra, K.D. Saha and C. Sinha, *Dalton Trans.,* 2017, **46**, 9245-9252.

(S6) A.K. Adak, B. Dutta, S.K. Manna and C. Sinha, *ACS omega*, 2019, **4**, 18987-18995.

(S7) A. K. Bhanja, S. Mishra, K. Kar, K. Naskar, S. Maity, S. Das, K. Saha and C. Sinha, *New J. Chem.*, 2018*, **42**, 17351−17358.

(S8) A. K. Adak, R. Purkait, S. K. Manna, B. C. Ghosh, S. Pathak and C. Sinha, *New J. Chem.*, 2019, **43**, 3899−3906.

(S9) Q. Liu, C. Liu, S. Cai, S. He, L. Zhao, X. Zeng and J. Gong, *Dalton Trans*., 2022, **51**, 3116−3121.

(S10) X. P. Zhang, Q. Yuan, Y. L. Qi, D. J. Zheng, Q. X. Liu, B. Z. Wang, Y. S. Yang and H. L. Zhu, *Spectrochim. Acta, Part A*., 2019**, 220**, 117134.

(S11) M. J. Frisch, G. W. Trucks, H. B. Schlegel, G. E. Scuseria, M. A. Robb, J. R. Cheeseman, G. Scalmani, V. Barone, B. Mennucci, G. A. Petersson and H. Nakatsuji, Fox. Gaussian 09 (Revision E. 01). Gaussian. Inc., Wallingford, CT, 2009.

(S12) A. D. Becke, *J. Chem. Phys.,* 1993, **96**, 2155-2160.

(S13) R. Bauernschmitt and R. Ahlrichs, *Chem. Phys. Lett.,* 1996, **256**, 454–464.

(S14) R. E. Stratmann, G. E. Scuseria and M. J. Frisch, *J. Chem. Phys.,* 1998, **109**, 8218–8224.

(S15) M. E. Casida, C. Jamorski, K. C. Casida and D. R. Salahub, *J. Chem. Phys.,*1998, **108**, 4439–4449.

(S16) N. M. O'boyle, A. L. Tenderholt and K. M. Langner, *J. Comput. Chem.,* 2008, **29**, 839–845.

(S17) Z. Li, Z. Zhan and M. Hu, Modulating Crystalline Structure of Metal-Organic Frameworks. *CrystEngComm.,* 2020, **22**, 6727-6737.

(S18) M. H. Mir, S. Bera, S. Khan, S. Maity, C. Sinha and B. Dutta, *Chem. Commun.,* 2021, **57**, 6197−6200.

(S19) B. Dutta, S. Bera, G. Bairy, M. Shit, C. Sinha and M. H. Mir, *ES Energy Environ*., 2022, **16**, 74−81.

(S20) S. Sanda, S. Parshamoni, S. Biswas and S. Konar, *Chem. Commun*., 2015, **51**, 6576−6579.

(S21) S. Bhunia, D. Sahoo, S. Maity, B. Dutta, S. Bera, NB. Manik and C. Sinha, *Inorg. Chem.,* 2023, **62**, 11976-11989.

(S22) P. Chakraborty, A. Rana, S. Mukherjee and S. Biswas, *Inorg. Chem*., 2022, **62**, 802-809.

(S23) J. Mandal, A. Dey, S. Sarkar, M. Khatun, P. Ghorai, P. P. Ray, P. Mahata and A. Saha, Inorg. Chem., 2024, **63**, 4527–4544.

(S24) G. Bairy, P. Das, B. Dutta, S. Bhowmik, P. P. Ray and C. Sinha, Inorg. Chem., 2023, **62**, 12773–12782.

(S25) S. Saha, M. Das, K. S. Das, R. Datta, S. Bala, J. L. Liu, P. P. Ray and R. Mondal, Crystal Growth Des., 2023, **23**, 1104–1118.

(S26) S. Bhunia, D. Sahoo, B. Dutta, S. Maity, N. B. Manik and C. Sinha, Inorg. Chem., 2023, **62**, 20948–20960.

(S27) S. Paul, B. Dutta, P. Das, S. Halder, M. Shit, P. P. Ray, K. Jana and C. Sinha, Appl. Organomet. Chem., 2023, **37**, e7160.

(S28) S. Khan, P. Das, S. Naaz, P. Brandão, A. Choudhury, R. Medishetty, P. P. Ray and M. H. Mir, Dalton Trans., 2023, **52**, 17934-17941.

(S29) S. Naaz, P. Das, A. Frontera, B. Dutta, S. Khan, P. P. Ray and M. H. Mir, Cryst. Growth Des., 2022, **22**, 5189-5197.

(S30) P. Ghorai, A. Dey, P. Brandão, S. Benmansour, C. J. Gómez García, P. P. Ray and A. Saha, Inorg. Chem., 2020, **59**, 8749-8761.

(S31) B. Dutta, A. Dey, C. Sinha, P. P. Ray and M. H. Mir, Inorg. Chem., 2019, **58**, 5419-5422.

(S32) K. S. Das, B. Pal, S. Saha, S. Akhtar, A. De, P. P. Ray and R. Mondal, Dalton Trans., 2020, **49**, 17005-17016.

(S33) S. Islam, P. Das, S. Maiti, S. Khan, S. Maity, P. Ghosh, A. D. Jana, P. P. Ray and M. H. Mir, Dalton Trans., 2020, **49**, 15323-15331.

(S34) S. Islam, J. Datta, F. Ahmed, B. Dutta, S. Naaz, P. P. Ray and M. H. Mir, New J. Chem., 2018, **42**, 13971-13977.

(S35) K. Naskar, A. Dey, S. Maity, P. P. Ray, P. Ghosh and C. Sinha, Inorg. Chem., 2020, **59**, 5518-5528.

38